A risk assessment framework for the socio-economic impacts of electricity transmission infrastructure failure due to space weather: An application to the UK

Edward J. Oughton[1,8*], Mike Hapgood[2], Gemma S. Richardson[3], Ciarán D. Beggan[3], Alan W.P. Thomson[3], Mark Gibbs[4], Catharine Burnett[4], C. Trevor Gaunt[5], Markos Trichas[6], Rabia Dada[7] and Richard B. Horne[8]

[1]University of Oxford, Oxford, UK,
[2]Science and Technologies Facilities Council, Harwell, UK,
[3]British Geological Survey, Edinburgh, UK,
[4]UK Met Office, Exeter, UK,
[5]University of Cape Town, Cape Town, South Africa,
[6]Airbus Defence and Space, Stevenage, UK,
[7]University of Cambridge, Cambridge, UK,
[8]British Antarctic Survey, Cambridge, UK.

* Corresponding author: Edward.oughton@ouce.ox.ac.uk at the Environmental Change Institute, University of Oxford, South Parks Road, Oxford, OX1 3QY

ACKNOWLEDGEMENTS

EO was supported by the Engineering and Physical Sciences Research Council via the programme grant Multi-scale Infrastructure Systems Analytics (Mistral) (EP/N017064/1). MH is supported by the Science and Technology Facilities Council. CB, GR and AT were supported by Natural Environment Research Council grant Space Weather Impacts on Ground-based Systems (SWIGS) (NE/P017231/1). RH was supported by the Natural Environment Research Council National and Public Good activity grant NE/R016445/1. TG and the GIC-effects group at UCT were supported by the Open Philanthropy Project. The authors would like to thank Andrew Richards, David Boteler and Daniel Ralph for their guidance in the development of the research.

ABSTRACT

Space weather phenomena have been studied in detail in the peer-reviewed scientific literature. However, there has arguably been scant analysis of the potential socio-economic impacts of space weather, despite a growing grey literature from different national studies, of varying degrees of methodological rigour. In this analysis, we therefore provide a general framework for assessing the potential socio-economic impacts of critical infrastructure failure resulting from Geomagnetic Disturbances, applying it to the British high-voltage electricity transmission network. Socio-economic analysis of this threat has hitherto failed to address the general geophysical risk, asset vulnerability and the network structure of critical infrastructure systems. We overcome this by using a three-part method which includes (i) estimating the probability of intense magnetospheric substorms, (ii) exploring the vulnerability of electricity transmission assets to Geomagnetically Induced Currents, and (iii) testing the socio-economic impacts under different levels of space weather forecasting. This has required a multidisciplinary approach, providing a step towards the standardisation of space weather risk assessment. We find that for a Carrington-sized 1-in-100-year event with no space weather forecasting capability, the GDP loss to the UK could be as high as £15.9 billion, with this figure dropping to £2.9 billion based on current forecasting capability. However, with existing satellites nearing the end of their life, current forecasting capability will decrease in coming years. Therefore, if no further investment takes place critical infrastructure will become more vulnerable to space weather. Additional investment could provide enhanced forecasting, reducing the economic loss for a Carrington-sized 1-in-100-year event to £0.9 billion.

KEY WORDS: Space weather; critical infrastructure failure; socio-economic impact assessment

SOCIAL MEDIA ABSTRACT

The economic impact of a 1-in-100-year space weather event to the UK could be as high as £16 billion. Enhanced space weather forecasting, could reduce this to £0.9 billion.

1. INTRODUCTION

Space weather can cause direct disruption to Critical National Infrastructure (CNI), including electricity transmission, satellite communications and Global Navigation Satellite Systems, aviation and rail transportation (Riley et al. 2018). Cascading failure can indirectly lead to the disruption of other essential systems. Space weather forecasting is essential to ensure CNI operators have time to implement operational mitigation measures to protect critical systems, reducing potential negative consequences. Yet, evidence on our shared global vulnerability to space weather, the potential socio-economic impacts of CNI service disruption, and the effect of different forecasting capabilities is still limited, despite this being essential (Schrijver et al. 2015). Internationally, there is now a new push to develop space weather mitigation strategies, especially in North America and Europe, as illustrated by President Obama's 2016 Executive Order (White House, 2016) or the UK's Space Weather Preparedness Strategy (Cabinet Office & DBIS, 2015). This has prompted the need for increased risk analysis of space weather threats (North, 2017).

Space weather includes multiple solar eruptive phenomena, including Coronal Mass Ejections (CMEs), Solar Energetic Particles and bursts of electromagnetic radiation (also known as 'solar flares'). We focus here on the impact of CMEs, consisting of billions of tonnes of electrically charged particles, carrying a magnetic field, ejected from the Sun into the interplanetary space (Webb & Howard, 2012). Extreme geomagnetic 'storms' can arise when large (10^{12}kg), dense (100 particles/cm^3) and fast (>500kms^{-1}) CMEs couple with Earth's magnetic field, particularly when the CME carries a significant southward-pointed direction ('B_z') magnetic field (Balan et al. 2014; Möstl et al. 2015; Temmer & Nitta, 2015). One significant terrestrial impact of space weather is that they drive large geomagnetic storms and their associated magnetospheric 'substorms', which produce intense and rapidly varying ionospheric currents. The generation of Geomagnetically Induced Currents (GIC) that follows from such rapid changes in Earth's magnetic field can pose a risk to the electrical power transmission network, as GIC flow from and to grounding points at transmission substations leading to the partial saturation of transformers (Boteler & Pirjola, 2014; Kappenman, 1996; Molinski, 2002; Viljanen & Pirjola, 1994).

While there has been considerable research published in the scientific peer-reviewed literature on the likelihood and severity of space weather phenomena, few studies have undertaken rigorous and robust quantification of the socio-economic impacts of space weather (Eastwood et al. 2017). This has left many scientists and other risk analysts feeling dissatisfied with the level of analysis presented in the grey literature. Our contribution is to provide a method that overcomes some of the limitations of previous analyses (Oughton et al. 2016; Oughton, Skelton, Horne, Thomson and Gaunt, 2017; Schulte in den Bäumen, Moran, Lenzen, Cairns and Steenage, 2014). This includes properly capturing (i) geophysical risk resulting from combined space and solid Earth physics, (ii) properties of infrastructure assets and (iii) the network structure of the high-voltage power grid. This information is then used to quantify the potential socio-economic impacts of space weather due to failure in electricity transmission, under different space weather forecasting capabilities. Both short-term power outages due to voltage instability, and long-term power outages due to transformer damage from thermal heating, are considered.

The research questions we investigate include:

1. What is the probability of CNI being affected by intense magnetospheric substorms?
2. How vulnerable are specific electrical transmission CNI assets and nodes to GIC exposure during intense substorms?
3. What are the potential socio-economic impacts of electrical transmission CNI failure due to space weather, under different forecasting capabilities?

In the following section, a literature review is undertaken. In Section 3 the method is articulated, with the results being presented in Section 4 and discussed in Section 5. Final conclusions are provided in Section 6.

2 LITERATURE REVIEW

Space weather is a high impact, low frequency (HILF) event. One of the most notable geomagnetic storms is known as the ‘Carrington Event’ of September 1859 and has been the focus of many scientific studies (e.g. Boteler, 2006; Green & Boardsen, 2006; Ribeiro, Vaquero and Trigo, 2011; Saiz, Guerrero,

Cid, Palacios, Cerrato, 2016; Silverman, 2006; Siscoe, Crooker and Clauer, 2006; Tsurutani, Gonzalez, Lakhina and Alex, 2003). However, data from this period are limited, giving rise to considerable diversity in the estimates of the size of the event. Within the digital age, the two key events studied include the March 1989 and October-November 2003 severe magnetic storms. During the severe 1989 geomagnetic disturbance (GMD), the Hydro-Quebéc power grid experienced a voltage collapse leaving six million customers without power for almost nine hours before the supply was restored (Barnes & Dyke, 1990). In July 2012, a very large and fast CME was observed by spacecraft but missed Earth. Estimates indicate this storm could have been Carrington-sized had it hit Earth (Baker et al. 2013).

2.1. Frequency and severity

Geomagnetic activity is often studied using extreme value statistics (Lotz & Danskin, 2017; Rodger et al. 2017; Thomson, Dawson and Reay, 2011). However, there are limited time-series data on which to understand both the frequency and severity of large events (Hapgood, 2011). Therefore, with only a limited catalogue of actual events, analysts often rely on extrapolations of power law or lognormal distributions to estimate extremes. For example, Riley & Love (2017) estimate the probability of an extreme event comparable to Carrington taking place in the next decade is 10.3% using a power law distribution and 3% using a lognormal distribution. Analysis by Kataoka (2013) estimates the probability of occurrence of extreme geomagnetic storms as a function of the maximum sunspot number of a solar cycle, with the probability of a Carrington-sized storm being 4-6% over the next decade. Jonas, Fronczyk and Pratt (2018) apply a Bayesian Model Average to the estimates of Riley (2012), Roodman (2015) and Love, Rigler, Pulkkinen and Riley (2015), to develop probabilities of space weather events of different intensities, finding an estimated 37% likelihood for an event comparable with March 1989 over a 10-year period. Due to data limitations, estimates for a Carrington-sized event are far more uncertain, ranging from approximately 1-10% over a 10-year period. Finally, Thomson et al. (2011) assess horizontal geomagnetic field changes finding that a typical mid-latitude (55-60º north) European observatory may experience a 1-minute peak rate-of-change in the field reaching 1000-4000 (1000-6000) nT/minute once every 100 (200) years.

2.2. The impact of GIC on electricity transmission infrastructure

GICs are correlated with and well characterised by the time derivative (rate-of-change, dH/dt) of the horizontal component (*H*) of the magnetic field (Bolduc, Langlois, Boteler and Pirjola, 1998). Effective parameterisation and prediction of GIC is challenging, requiring information on ground conductivity and magnetic field variations in relation to the exposed power grid structure (Boteler, 2014). Comprehensive analyses of the current understanding of space weather GIC hazards to power grids can be found in Gaunt (2016) and Pulkkinen et al. (2017).

The most significant effects of GICs on power systems derive from the nonlinear magnetic core response of a transformer to GIC (Bolduc, Gaudreau and Dutil, 2000; Boteler, Shier, Watanabe and Horita, 1989). As the core is driven into partial saturation by the low frequency GIC (with effects similar to those of direct current), the transformer exhibits some of the characteristics of an inductor or reactor in the power circuit; the reactive power drawn by the transformer increases (approximately in proportion to its power rating and the GIC present) and a power frequency current higher than the normal current flows in the transformer, with three main effects. Firstly, the heat 'generated' by losses inside the transformer causes its temperature to rise (Marti, Rezaei-Zare and Narang, 2013), even to the extent of initiating damage to the winding conductors or paper insulation or the breakdown of the oil, with the result that the automatic protection removes (trips) the transformer from the system. Secondly, the increased current causes the voltage drop in all lines to increase, possibly to the point that the voltage cannot be sustained by the automatic tap changers on the transformers, and the system switches off to protect itself from the abnormally low voltages and high currents. As the voltages fall, the effectiveness of shunt capacitors (used for voltage support) falls too, so the response of the system to the GIC-reactive power combination is, again, not linear, potentially leading to voltage collapse. Finally, the increased current, which has a high harmonic content because of a transformer's non-linear response, can trip an overcurrent protection relay, or the harmonics may cause the correct or incorrect operation of other types of relays, removing important components from the system, including lines and shunt capacitor banks. These protection relay operations, including the tripping of a damaged transformer, can cause localised loss of supply and aggravate the possibility of voltage collapse (Albertson, Thorson and Miske, 1974). In addition to these effects, the harmonic distortion propagates into the distribution

networks and can affect negatively the performance of customers' electrical and electronic equipment (Schrijver, Dobbins, Murtagh and Petrinec, 2014).

2.3. Space weather socio-economic impacts

The key dimensions of the literature on the socio-economic impacts of space weather have been highlighted in Table I. We particularly emphasise whether different studies include data-derived ground conductivity risk, asset vulnerability and network structure because this has generally been a limitation.

A frequently referenced study by Lloyd's of London (2013), assessed the risk to the North American electricity grid, estimating that the potential total cost for a scenario where 20-40 million people were left without power for between 16 days to 1-2 years, could range from $0.6-2.6 trillion USD. In a cost-benefit analysis of the European Space Agency's (ESA) Space Situational Awareness programme, PwC (2016) estimated the GDP impact of a space weather-induced blackout to be approximately €5.7 billion, predicated on a three-day blackout taking place in three major European cities.

Within the peer reviewed literature, Schulte in den Bäumen et al. (2014) analysed the global consequences of severe space weather on East Asia, Europe and North America, finding that a Quebec 1989-like event could see a global economic impact of $2.4 – 3.4 trillion over a year, leading to a global GDP loss of 3.9-5.6%. In a study focusing just on the USA, Oughton et al. (2017) estimated the daily loss from electricity transmission failure for the USA based on different geomagnetic storm footprints, finding that it could range from $7-42 billion.

Table I. Literature review of existing space weather impact assessments

Year	Author	Geography		Spatio-temporal impacts		Ground conductivity data?	Asset vulnerability ?	Explicit Network structure?	Economic method	Economic impact				Formally Peer Reviewed?
		Country	Region	Population affected	Restoration period					Asset damage	Direct economic impact	Indirect economic impact	Total economic impact	
1990	Barnes & Dyke	USA	North East	Not stated	50% connected in 16 hours, 75% in 24 hours, 100% in 48 hours	No	No	No	Value of Lost Load estimation	$16 million (1988 USD)	$3-6 billion (1988 USD)	Not modelled	Not modelled	Yes
2002	Bolduc	Canada	Quebec	9 million	N/A	No	No	No	Not stated	$13.2 million (CAN dollars)	Not modelled	Not modelled	Not modelled	Yes
2005	Pulkkinen, Lindahl, Viljanen and Pirjola	Finland	Malmö	50,000	1 hour	No	No	No	Not stated	Not stated	$0.5 million (USD)	Not modelled	Not modelled	Yes
2008	Kappenman (in Space Studies Board)	USA	National	Not stated	4 to 10 years	Yes	Yes	Yes	Not stated	Not stated	$1-2 trillion (USD)	Not stated	Not stated	No
2013	Lloyd's of London	North America	N/A	20-40 million	16 days to 1-2 years	Yes	Yes	Yes	Value of Lost Load estimation	Not stated	$0.6-2.6 trillion (USD)	Not modelled	Not modelled	No
2014	Schulte in den Bäumen et al.	Global	National	Not stated	5 months to 1 year	No	No	No	Multi-Regional Input-Output analysis	Not modelled	Not stated	Not stated	$3.4 trillion (USD)	Yes
2014	Schrijver et al.	North America	National assessment	N/A	N/A	N/A	N/A	N/A	Retrospective cohort exposure study	Not stated	~4% of claims are statistically associated with geomagnetic activity	Not modelled	Not modelled	Yes
2016	PwC	Europe	N/A	'3 cities'	3 days	No	No	No	Input-Output analysis	€0.26-0.31 billion	€2-2.7 billion	€1.7-2.1 billion	€3.7-4.8 billion	No
2017	Oughton et al.	USA	National assessment	8-66%	24 hours	No	No	No	Multi-Regional Input-Output analysis	Not modelled	$3-28.2 billion (USD)	$1.4-7.2 billion (USD)	$4.4-35.4 billion (USD)	Yes
2017	Abt Associates	North America	National assessment			No	No	No	Value of Lost Load estimation	Not stated	Not stated	Not stated	~$0.4-10 billion (moderate), $1-20 billion (extreme)	No

Very few studies have assessed the potential ramifications of space weather forecasting. One rare example by Teisberg & Weiher (2000) find that the net benefits of a satellite warning system are strongly positive, and having undertaken a sensitivity analysis, remain positive even if the damage is as low as $2 billion. Enhanced space weather forecasting capability has the potential to (i) increase the warning time prior to an event taking place, and (ii) increase the confidence in the forecast, reducing the probability that the warning will be ignored (for a discussion of the cost-loss implications of space weather forecasting see Henley & Pope, 2017). Three key actions that can be enabled include implementation of infrastructure operator mitigation plans, business continuity plans, and local building and community resilience activities. The key action in this case is the ability for CNI operators to engage emergency mitigation plans earlier, helping to prevent both damage to key assets and potential loss of human life following CNI disruption.

3. METHOD

A general assessment framework is developed for the UK. We test specific Geomagnetic Disturbances GMD, which are a threat to the system of study, referring to different variations as $GMD_1, \dots, GMD_z$ with each scenario representing a different level of threat manifestation (1-in-10-year, 1-in-30-year, and 1-in-100-year). Specifically, in our study scenario GMD_i signifies that during event i, m Extra High Voltage (EHV) transformers (≥275kV) in a transmission substation node (n) within the network could have failed due to GIC exposure. Hence, each n node contains multiple transformers $m_1, \dots, m_z$ with each transformer having a set of technical characteristics $c_1, \dots, c_z$, indicating that each transformer type has a different level of vulnerability to GIC. Thus, for a comprehensive vulnerability assessment of each space weather event GMD_i we simulate failure possibilities in the system, giving rise to a set of failure scenarios $S_1, \dots, S_d$. The impact of each scenario is initially measured in terms of the proportion of directly affected consumers $cs_1, .., cs_i$ and directly affected labour $ls_1, .., ls_i$ at each node. Consequently, the level of disruption is estimated based on electricity loss for a set of event scenarios $S_1, .., S_h$ and is quantified using lost Gross Domestic Product (GDP). Fig. 1 illustrates the framework applied to the UK.

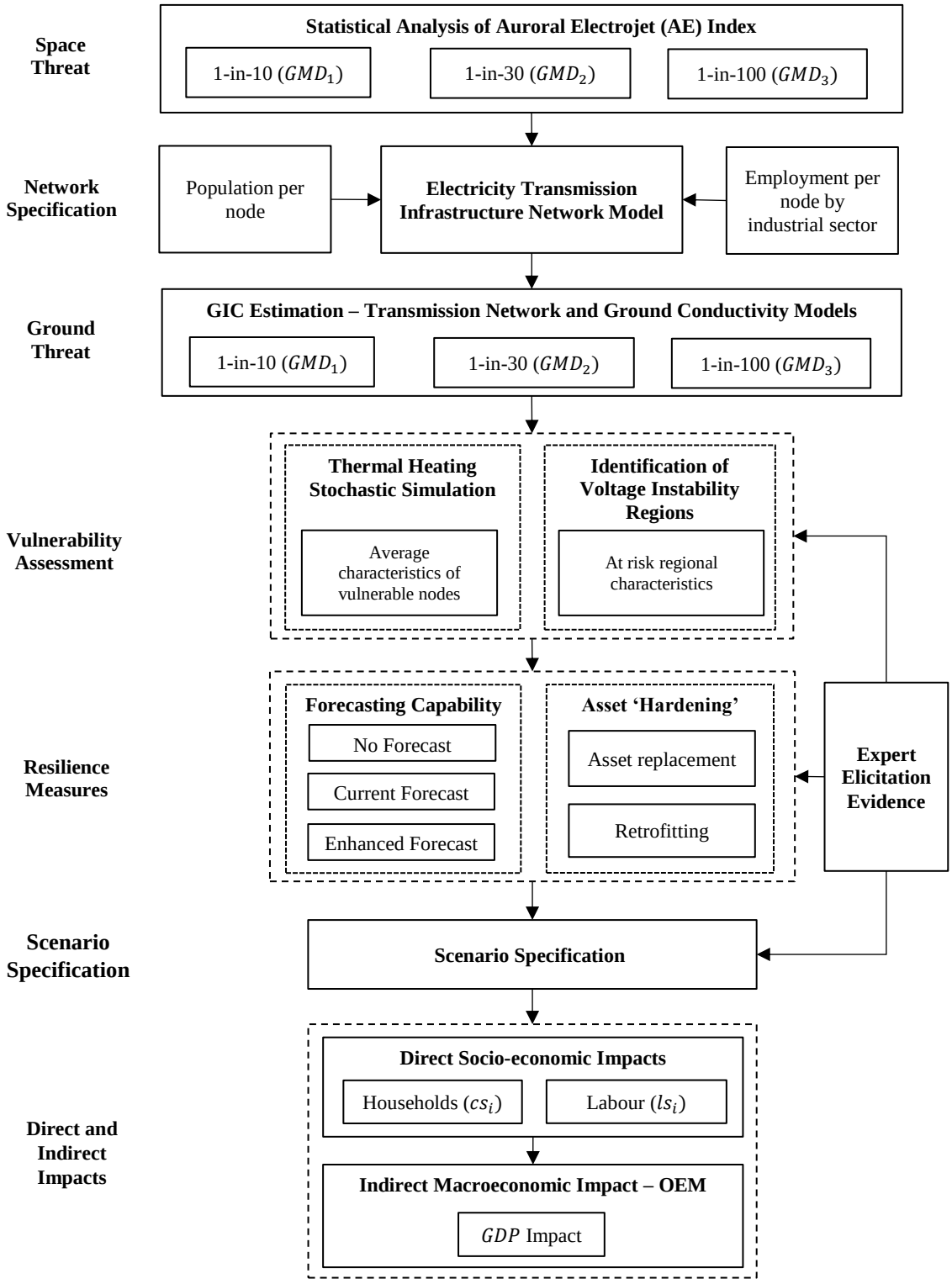

Fig. 1. Assessment framework

3.1. Space threat

We construct GMD scenarios that are time sequences of substorms of differing intensities. These sequences are based on the Auroral Electrojet (AE) geomagnetic activity index (Davis & Sugiura, 1966), sourced from the UK Solar System Data Centre. We use data from 28-29th October 2003 to construct a 1-in-10-year scenario (GMD_1) and 13-14th March 1989 to construct a 1-in-30-year scenario (GMD_2). In each case we smooth the AE data by taking a 31-minute running median (to suppress short-lived spikes in the data), and identify substorms as distinct peaks in the smoothed data. We focus on the most intense peaks with AE>1500nT, as only these are considered to have potentially significant impacts, and we describe these peaks as "very intense substorms". For the purposes of this study, we use a conservative assumption that the potential impact maximises if the substorm occurs around 01:00–03:00 local time at the grid location. This is consistent with the voltage collapse of the Quebec grid (Bolduc, 2002) which occurred during a very intense substorm around 03:00 local time on 13th March 1989. Appendix A provides a detailed methodological note on this procedure.

To construct a 1-in-100-year scenario (GMD_3), data are adapted from the 1989 storm to match key features of the Carrington event of 1859 which comprised two geomagnetic storms, (i) a very large storm with a Sudden Storm Commencement (SSC) around 05:00UTC on 2nd September, preceded by (ii) a smaller but still large storm with an SSC around 22:30 UTC on 28th August (Stewart, 1861). These adaptations shift the SSC to the correct time of day and year, the former being the key change for the purposes of our analysis since, as discussed above, it determines when a power grid is in our risk window of 01:00–03:00 local time. Thus, to represent the 2nd September storm, the 1989 AE time series is time shifted so that the SSC in that series moves from 01:27UTC on 13th March to 05:00 on 2nd September. Additionally, AE values are added to represent the 28th August storm using another copy of the 1989 AE time series, but instead time-shifted so that the 1989 SSC moves to 22:30 on 28th August. We then overlay this subset, without any scaling, on to the first. The net result is a time series of simulated AE values covering 15 days around the Carrington event and including variations that we can consider representative of the two large storms recorded by Stewart (1861). We then apply median

smoothing and thresholding, as above, to derive a sequence of substorms that we use as our 1-in-100-year scenario (GMD_3).

We map the 1-in-100-year scenario into grid impacts by assuming, as above, that this maximises where the local time is 01:00–03:00 at the time of the substorm. This leads to major impacts in North America, consistent with the many reports that the Carrington event generated intense aurora over North America (Green & Boardsen, 2006). It also generates major impacts in Australia, New Zealand and Japan, China and parts of Russia. However, it does not generate very severe impacts over Western Europe, due to the SSC timing matching the Carrington event. The scenario is expanded to consider a full 24-hour range of SSC times to reflect CMEs arriving at Earth at different times of day. This is achieved by varying the SSC in one-hour steps from 0-23hrs and varying the footprints westward by 15° at each step. Thus, we generate 24 different scenarios for each risk level and can estimate how many lead to very intense substorms over the UK. The results offer evidence for each return period to answer the first research question, as well as provide contextual information to inform the scenario specification.

3.2. Electricity transmission infrastructure network model

The British high-voltage transmission power grid consists of a 275 kV and 400 kV transmission network (we exclude the higher resistance 132kV Scottish lines). A detailed description of the British high-voltage power network is developed using public information from the National Grid Electricity Ten Year Statement released in 2016, augmented by an extensive search of online maps and satellite imagery. This network model consists of latitude, longitude, and certain electrical characteristics (earthing, transformer and line resistances) of each substation node and line in the network; the 2016 model has 307 grounded nodes and 519 lines. Some connections are very short, for example, between two transformers on the same site, while the longest is 189.5 km. The median line length is 15 km (mean: 22km). In the absence of a local distribution network model, we affiliate the local population to the nearest grid node, as illustrated in Fig. 2(A). The structure of the high-voltage networks for Britain are illustrated in Fig. 2(B), along with the total and EHV-only transformer assets per node (C and D respectively).

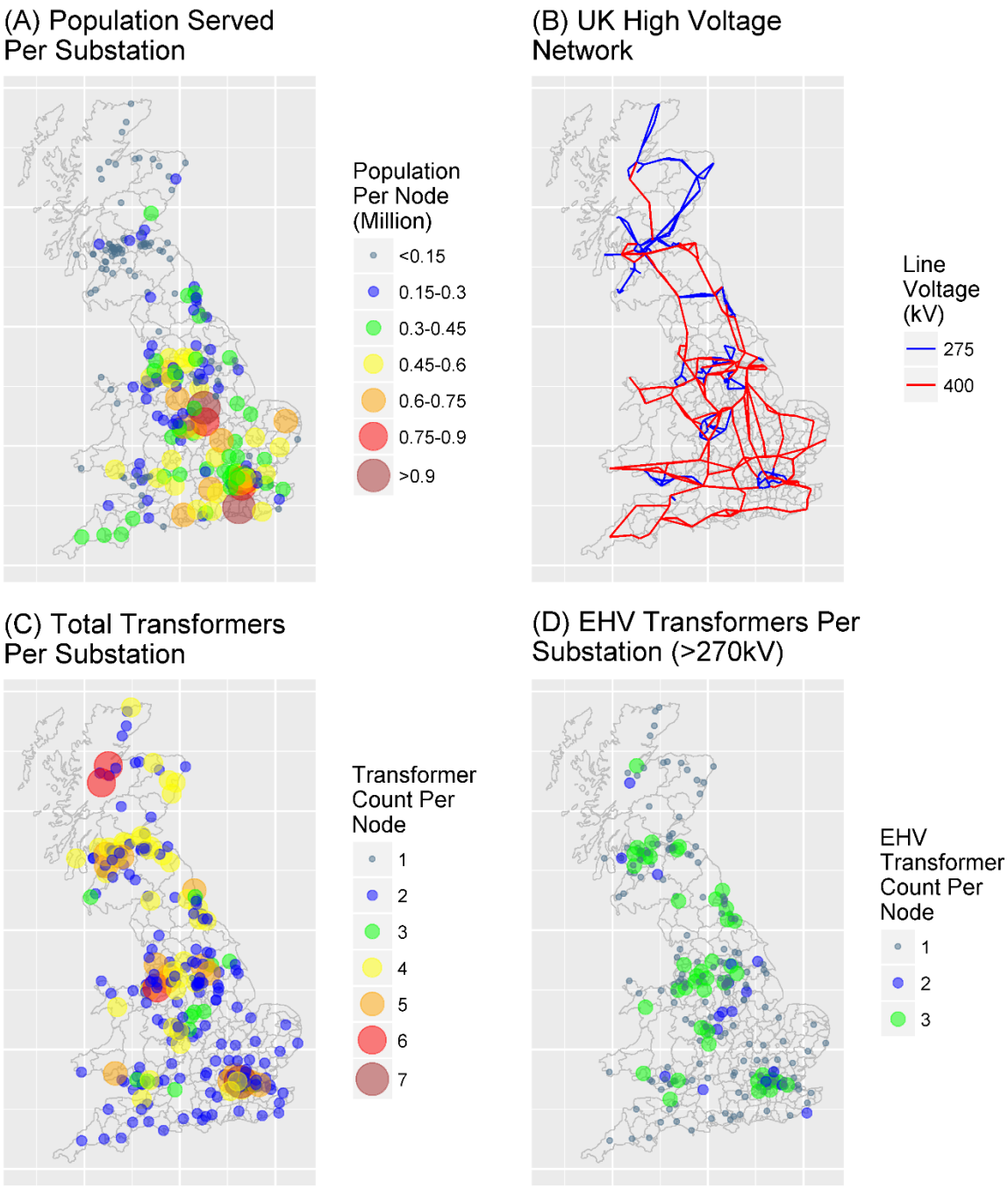

Fig. 2(A) Population served per substation, (B) British high-voltage network, (C) total transformers per substation and (D) EHV transformers per substation

The statistical data from ONS (2016) are used in this process, consisting of 7,201 Middle Output Areas for England and Wales, and 1,279 Intermediate Data Zones for Scotland. Hence, this leads to a total of 8,480 statistical areas. Employment data are also obtained via the open-access Business Register and Employment Survey, and simplified from eighteen broad industrial groups to nine.

3.3. Ground threat

To generate a realistic representation of the spatial variation of the geomagnetic field during a large storm, a model of the largest digitally measured magnetic field events (October 2003, for the 1-in-10-year storm, and March 1989, for the 1-in-30-year, or rarer, storm) is constructed based upon measurements from five geomagnetic observatories. Appendix B provides a detailed method on the GIC estimation and validation procedures utilised.

Using (scaled) magnetic field data and a UK-specific Earth conductivity model, a map of the geoelectric field is generated for every minute of the two events. This is then combined with the electricity transmission infrastructure network model to determine GIC per node. If the ground resistance is sufficiently high, the low-resistance wires of the network offer an easier route for GIC to pass through the earthed neutrals of the connecting transformers, essentially creating a short-circuit. In some cases, there are insufficient data to determine the earthing resistance, so we have assumed this to be 0.5 Ω (Kelly, Viljanen, Beggan and Thomson, 2017). These network parameters are used to calculate GIC (in Amperes) along power transmission lines according to Lehtinen & Pirjola (1985):

$$\boldsymbol{I} = (\mathbf{1} + \boldsymbol{Y} \cdot \boldsymbol{Z})^{-1} \cdot \boldsymbol{J} \qquad 1$$

where $\boldsymbol{J}$ is the 'perfect earthing' current (the geo-voltage computed between nodes divided by the connecting line resistances), $\boldsymbol{Z}$ is the impedance matrix, $\boldsymbol{Y}$ is the network admittance matrix and $\boldsymbol{I}$ is the vector containing the estimated GIC at each node. The input data from the network parameters are used to calculate $\boldsymbol{Y}$ and $\boldsymbol{Z}$. The geo-voltage for $\boldsymbol{J}$ is calculated by interpolating the electric field grid value onto the power transmission lines and integrating along the line. The GIC at each node on the grid are then computed, calculated from the sum of both the North and East components of the surface electric field. The method for the calculation of GIC in the British network has been benchmarked against Horton, Boteler, Overbye, Pirjola and Dugan (2012) in Richardson & Beggan (2017), by ensuring that the GIC values produced by the model code are consistent for the given grid, and thus are valid.

The Dst index is a measure of the severity of a GMD based on ring current intensification. For the 1-in-10-year event we use the Dst magnitude for 2003 (-383nT) (Echer, Gonzalez and Tsurutani, 2008)

(GMD_1) and for the 1-in-30-year (GMD_2) we use 1989 (-589nT) (Allen et al. 1989). These return periods are supported by Jonas et al. (2018). Since we expect more intense auroral currents in larger GMDs, GIC values from 1989 may be scaled to reflect more severe events. The Dst of the Carrington event was originally estimated as -1760 nT (Tsurutani et al. 2003). This estimate was based on a short-duration (half-width ~40 minutes) dip of 1600 nT in the horizontal magnetic field intensity measured at Mumbai during the 1859 storm. Siscoe et al. (2006) re-analysed these data using standard procedures for Dst derivation, e.g. hourly averaging, and derived a value of -850 nT for the minimum Dst of the Carrington event. This latter value has now been widely adopted in assessments of the Carrington event (e.g. Pulkkinen, Bernabeu, Eichner, Beggan and Thomson, 2012; Riley & Love, 2017), and produces a scaling factor of x1.4 for a 1-in-100-year event (GMD_3), though Cliver & Dietrich (2013) propose a range from -850 to -1050 nT. In this paper we take a conservative approach and use the -850 nT value derived by Siscoe et al. (2006). There is a level of uncertainty in these estimates, as reflected in Jonas et al. (2018), however exploring further event sizes is beyond the scope of this paper.

For the vulnerability analysis, we also include additional extreme scenarios for exploratory purposes. This also helps emphasise the uncertainty arising from extrapolating Dst and the return time. Following Jonas et al. (2018:4), a 1-in-500-year event is estimated to correspond to Dst of -1400nT, producing to a scaling factor of x2.4, and a 1-in-1,000-year event has an approximate Dst of -1800nT resulting in a scaling factor of x3.1. Finally, Vasyliūnas (2011) proposes a *theoretical upper limit* for the largest geomagnetic storm possible corresponding to a Dst of -2500nT, which we utilise as an example of equivalent to a '1-in-10,000-year' event, with a scaling factor of x4.2.

3.4. Vulnerability assessment

In this section we describe the method for undertaking a vulnerability assessment of transmission infrastructure assets and nodes to thermal heating and voltage instability. Regarding thermal heating, we develop a stochastic simulation model whereby the probability of transformer failure scales based on GIC exposure per transformer. Failure is defined as the complete interruption of part of the electricity system.

Two routes to failure are considered. Firstly, transformer damage can result from thermal heating which subsequently prevents the asset carrying out normal functionality, requiring an inspection and component replacement, or potentially replacement with an on-site or off-site spare prior to reconnection. This route to failure represents a long-term power outage, whereby assets affected in this way take weeks to restore to normal service. Secondly, automatic or manual protection removes transformer assets from active operation as a result of voltage instability, requiring a physical inspection before being returned to service. This route to failure represents a short-term power outage, whereby assets affected in this way can be returned to service in a matter of hours or days. We assume that the instantaneous peak GIC per node is of sufficient amplitude and temporal duration to cause transformer asset failure during each intense substorm. The results generated are utilised in the scenarios tested later in this paper.

After the severe 1989 space weather event, the UK transmission grid operator introduced improved hardening measures for new transformer assets capable of being exposed to higher GIC exposure thresholds, commencing with transformer procurements made in 1999. However, due to the asset replacement cycle taking multiple decades these protections are not yet fully pervasive. Data on the transformer fleet characteristics (including high and lower voltage-side resistances and earthing arrangements) are commercially sensitive and hence unavailable for this analysis. Therefore, we reflect these existing asset hardening measures by exploring the sensitivity of transformer failure based on the random allocation of this unknown parameter. Expert elicitation interviews with the operator provided information regarding four heterogeneous transformer types, each with a different set of technical characteristics, in which 50% are c_1 and can withstand 200A of GIC in the neutral, 25% are c_2 and can withstand 100A, 12.5% are c_3 and can withstand 50A, and 12.5% are c_4 and can withstand 25A. The probability of failure p_i for each transformer is thus scaled between the lower withstand threshold and a threshold 100A above, based on the GIC for the m transformer at each n node. Using the following scaling equation yields $0 \leq p_i \leq 1$ for transformer design characteristic types $c_1, \ldots, c_z$:

$$p_i = \frac{GIC_i - \min(c_z)}{\max(c_z) - \min(c_z)} \qquad 2$$

The results of this simulation provide a distribution based on the frequency of transformer failures. We also examine the frequency of n node failures, assuming this takes place if more than half of the m EHV transformers present fail. The simulation is run for 1,000 iterations and the resulting distributions on transformer and node failures provide average population and employment characteristics per node under each scenario.

Regarding voltage instability, we again utilise expert elicitation methods to identify zones at risk. Voltage instability is stated as being the most likely impact to the UK grid (Cannon et al. 2013). When large GICs enter and exit power transmission systems this phenomenon can cause a variety of reported problems including reactive power surges and system voltage dips leading to grid instability (Boteler et al. 1989). If the GICs produced are large enough, the system can no longer handle the reactive power being demanded, causing voltage collapse and a system-wide power outage (Hutchins & Overbye, 2011). The system operator considers the largest voltage instability risks to be present in key urban conurbations. This is due to the density of transformer assets and the losses associated with transmitting reactive power over long distances.

3.5. Resilience measures

There are a variety of resilience measures for space weather threats, including both forecasting and infrastructure 'hardening'. Some asset hardening has already taken place in the British grid and is partially reflected in the vulnerability analysis articulated in the previous section via heterogenous asset exposure thresholds. However, retrofitting existing transformers is expensive and not being contemplated at this stage in the UK. Hence, the emphasis of this paper is on UK space weather forecasting because it is a recognised resilience measure, enabling the advanced implementation of operational mitigations. This includes increasing generation capacity and reducing power transfer in heavily loaded lines (Bolduc, 2002).

Increasing total system generation capacity, reduces generation output below each specific transformer's rated level of operation, reducing normal operational heating and providing more capacity to absorb abnormal GIC exposure. This may be adequate to avoid GICs causing or initiating permanent

damage to a transformer. Decreasing power transfer on transmission lines, reduces line voltage drop and diminishes the risk of being exposed to voltage 'instability' or a classic voltage collapse of the power system. As the level of forecasting capability has a significant impact on our subsequent ability to deal with this risk, we therefore describe how this differs by scenario, using evidence gathered via expert elicitation in collaboration with the UK Met Office's Space Weather Operations Centre (MOSWOC). Appendix C provides a detailed overview of space weather forecasting capabilities.

In a *No Forecast* scenario, existing space weather satellite observing systems are not replaced prior to the end of their operational life or the scientific mission for which they were originally intended, leaving no coronagraphs available from the Solar and Heliospheric Observatory (SOHO) or the Solar Terrestrial Relations (STEREO) assets. This significantly reduces the forecasting capability and may in extremis render forecasting of severe space weather events useless. At present there are plans under consideration in the US that may lead to SOHO, the Deep Space Climate Observatory (DSCOVR) and the Solar Dynamics Observatory (SDO) being replaced by a mixture of operational and science missions, but no commitment has been made yet. Similarly, whilst planning is in progress within ESA, a decision on whether to replace the off Sun-Earth line, side-on view currently provided by STEREO is not expected until the end of 2019 at the earliest. Unlike STEREO, this mission would be permanently located close to the Lagrange L5 point, 60 degrees behind the Earth in its orbit. This is the optimal view for operational purposes as it enables continuous monitoring of solar active regions just before they are positioned to launch CMEs towards Earth.

In a *Current Forecast* scenario, this reflects the present forecasting capability, based on existing satellites, allowing forewarning of active regions on the Sun (3-4 days before CME arrival). Once a CME has launched SOHO and STEREO coronagraphs are available to support CME forecast arrival time within +/-6 hours, but the non-operational status of the spacecraft data results in delayed recognition of the potential threat level. Data gaps degrade the reliability and accuracy of forecasts.

In an *Enhanced Forecast* scenario, this reflects the standard that could be achieved if the current observations were supplemented by satellites on and off the Sun-Earth line with dedicated L1 and L5 spacecraft. This would allow a longer (6-7 day) forewarning of the complexity of an active region.

Coronagraphs, combined with an improved assessment of background solar wind would provide a much higher level of confidence in the CME arrival time (+/-4 hours). Moreover, a Heliospheric Imager would allow updates to be made to the arrival time during CME transit. Table II provides a detailed behavioural description for different forecasting capabilities by scenario.

Table II. Detailed description of space weather forecasting capability by scenario

	No Forecast	**Current forecast**	**Enhanced forecast**
1-in-100-year	Very challenging to discriminate between a minor event and a significant 1-in-100-year event. Therefore, infrastructure operators do not have sufficient confidence to implement operational mitigations.	Infrastructure operators implement their currently agreed operational mitigations. While this can help to partially mitigate the risk, poor confidence/accuracy in the forecast means mitigation is likely to be sub-optimal due to the associated cost of implementation.	The early identification of a complex active region allows infrastructure operators to fully implement a wider range of operational mitigations. Additional confidence in the arrival time increases the perception of the threat, providing a clearer cost/benefit ratio for operational mitigations. This partially results from a lower 'false alarm' rate.
1-in-30-year	Very challenging to discriminate between a minor event and a significant 1-in-30-year event. Unless there was evidence that it might be extreme, we assume that infrastructure operators decide not to implement operational mitigations.	Infrastructure operators do not fully implement currently agreed operational mitigations due to the expected levels of severity. While this can help to partially mitigate the risk, poor confidence/accuracy in the forecast means mitigation is likely to be sub-optimal due to the associated cost of implementation.	The additional lead time in identifying a complex active region allows NG longer to implement a wider range of mitigating actions. Additional confidence in arrival time increases the perception of the threat, providing a clearer cost/benefit to mitigating actions. This partially results from a lower 'false alarm' rate.
1-in-10-year	Very challenging to discriminate between a minor event and a significant 1-in-30-year event. Unless there was evidence that it might be extreme, we assume that infrastructure operators decide not to implement operational mitigations.	Infrastructure operators do not fully implement currently agreed operational mitigations due to the expected levels of severity. At this scale of event, it is envisaged that the risk would be effectively mitigated resulting in only minor impacts.	The early identification of a complex active region allows infrastructure operators to fully implement a wider range of operational mitigations. Additional confidence in the arrival time increases the perception of the threat, providing a clearer cost/benefit ratio for operational mitigations. This partially results from a lower 'false alarm' rate.

In both the Current Forecast and Enhanced Forecast capabilities, satellite missions need to be accompanied by investment to ensure computer models, systems and staff are in place to predict and communicate space weather.

3.6. Scenario specification

Scenario analysis is a foresight tool that enables the testing of exogenous shocks to a system of study. This technique enables the production of comparative analytics that support strategic decision-making. For a review of scenario approaches for risk analysis see Tosoni, Salo and Zio (2017). Where gaps exist in specifying scenario parameters because traditional scientific analysis is infeasible or not yet available, we utilise expert elicitation. This was undertaken based on information obtained from a co-organised workshop, and a set of detailed stakeholder interviews conducted with organisations responsible for critical infrastructure and associated risk management activities. The Space Weather and Critical Infrastructures workshop was held in Ispra, Italy (see Krausmann, Andersson, Gibbs and Murtagh, 2016), co-organised with Europe's Joint Research Centre, the Swedish Civil Contingencies Agency, UK Met Office and US NOAA's Space Weather Prediction Centre. Expert elicitation interviews were targeted with leading individuals across energy (4), aviation (2), transportation (2), satellite (3), insurance (4), government (9) and academia (4) to assess current exposure to space weather (number of interviewees in parentheses). Interviewees were asked to outline the key space weather threats they were concerned about, the expected spatial and temporal impacts of these threats, and the different mitigation strategies they currently utilise. Explicit information was gathered regarding the expected impact resulting from different levels of space weather forecasting. We consequently describe a set of evidence-based scenarios that combine (i) modelled outputs from the vulnerability assessment, (ii) evidence from the UK's National Risk Register, and where data are unavailable (iii) qualitative information obtained from expert elicitation.

Evidence gathered from the Royal Academy of Engineering report by Cannon et al. (2013), later used for the UK's National Risk Register, states that thermal heating could damage approximately 13 EHV transformers from a Carrington-sized event. This is the infrastructure operator's own assessment, and includes two substations experiencing catastrophic damage, leading to disconnection from the

transmission grid for potentially two to four months. This estimate is based on the transmission operator's own analysis, with full access to asset vulnerability, existing mitigation and knowledge of stock-piled transformers. Using this information, we consequently scale the restoration periods for different event sizes and forecasting capabilities via expert elicitation with the UK MOSWOC. As we do not explicitly know which nodes are most at-risk, we take the average population and employment characteristics of failed nodes, for each scenario, from the simulated vulnerability analysis. Additionally, voltage instability zones are identified using expert elicitation and are corroborated using transformer densities from the developed infrastructure model. Table III provides a description of each scenario by impact type. We assume a linear temporal restoration process for each scenario.

If no forecasting capability is available and multiple substorms are experienced, this dramatically increases the probability of a national voltage collapse. Therefore, we use this as the basis of the 1-in-100-year event if no forecasting capability is available. This situation would necessitate 'BlackStart' where the grid must be brought back online via plants capable of using onsite generators, taking up to five days (Cabinet Office, 2017). Damage is also caused to two network nodes requiring transformer replacement from an off-site location.

Table III. Scenario description based on event size and forecasting capability

Event	Impact Type	Dimension	No Forecast	Current Forecast	Enhanced Forecast
1-in-100-year	Voltage collapse	Spatial	National grid collapse	3 voltage instability regions	1 voltage instability region
		Temporal	5 days	2 days	1 day
	Thermal heating	Spatial	2 nodes	2 nodes	1 node
		Temporal	10 weeks (extended off-site transformer replacement)	6 weeks (off-site transformer replacement)	4 weeks (expedient off-site transformer replacement)
1-in-30-year	Voltage collapse	Spatial	2 voltage instability regions	1 voltage instability regions	-
		Temporal	2 days	1 day	-
	Thermal heating	Spatial	1 node	-	-
		Temporal	6 weeks	-	-
1-in-10-year	Voltage collapse	Spatial	1 voltage instability region	-	-
		Temporal	12 hours	-	-
	Thermal heating	Spatial	-	-	-
		Temporal	-	-	-

If the current forecast is available, interview evidence suggests that mitigation actions for a 1-in-100-year event would cause blackouts in a limited number of voltage instability regions. We assume this takes place in three regions as the auroral electrojet shifts equatorward, with one very intense substorm affecting Birmingham, and another affecting both the Manchester and Yorkshire regions. Two nodes require transformer replacement from an off-site location taking six weeks to complete. In an enhanced forecast scenario, a 1-in-100-year event may cause only limited short-term power loss to one voltage instability region such as Birmingham and the West Midlands. Damage from thermal heating could be limited to only a single node, and expedient off-site replacement of transformer assets could be carried out in four weeks. For the 1-in-30-year scenarios, the potential effects are limited, with an enhanced forecast leading to no impacts. Similarly, in the 1-in-10-year scenarios a worst-case would involve short-term blackouts in a single voltage instability region if no forecast was available, otherwise no impacts would take place (as is consistent with our current experience of space weather). We do not test scenarios for events less frequent than 1-in-100-years, due to the increased level of uncertainty.

3.7. Direct and indirect impacts

Direct impacts are measured by (i) the proportion of the population without power and (ii) local employment disruption by broad industrial group. Voltage instability impacts are calculated by aggregating population and employment within voltage instability regions. For thermal heating risk, we take the average node characteristics from failed nodes by scenario, over 1,000 simulation runs.

Secondly, we use the Oxford Economics Global Economic Model (OEM) to understand the impact on GDP. This is a widely employed macroeconomic model with users including the International Monetary Fund and World Bank. Multivariate forecasts are produced for many economies, but here we focus only on the UK. The modelling approach adopts Keynesian principles in the short run, and monetarist principles in the long run. The demand-side determines short-run output, while in the long-term supply-side factors determine output and employment. We quantify the indirect economic impact as 1-year deviation from baseline growth starting in Q1-2018, given a demand-side economic shock due to reduced private consumption from households being without power. Private consumption is affected as consumers are unable to complete daily economic transactions. We parametrise a private consumption shock cs_i based on the population disruption from both thermal heating PTH_{it} and voltage instability PVS_{it} at time t in the ith scenario as follows:

$$cs_i = \frac{(PTH_{it} + PVS_{it})}{P \cdot (\frac{w}{q})} \quad 3$$

where P is the total population (63.3 million), w is the number of working days per year (280) and q is the number of quarterly periods per year. This process is repeated for a quarterly supply-side labour shock ls_i to represent reduced labour supply, as employees are unable to travel to work or log in remotely. The summation of labour disruption from both thermal heating LTH_{it} and voltage instability LVS_{it} at time t in the ith scenario is as follows:

$$ls_i = \frac{(LTH_{it} + LVS_{it})}{L \cdot (\frac{w}{q})} \quad 4$$

Where the total labour force is represented by L (30.9 million), w is the number of working days per year (280) and q is the number of quarterly periods per year. The analysis focuses on the short-term GDP impacts, and not on the long-term equilibrium position of the economy. Finally, the model output for each scenario is subtracted from the baseline growth estimate, to obtain the GDP impact per scenario. The Global Economic Model utilised is available from Oxford Economics, obtained here under academic licence, and therefore is accessible for other analysts wishing to reproduce similar analyses. The model partially solves rescheduling and input substation effects over a 1-year period, but a longer-term analysis would more effectively quantify any rebound effects associated with post-disaster recovery.

4 RESULTS

4.1. Magnetospheric substorm probability

Following the method outlined in Section 3.1., we construct time sequences of substorms to quantify the uncertainty associated with the rotation of the Earth, and now report the magnetospheric substorm probability for each of the risk scenarios in Table IV. This shows how the likelihood of a very intense substorm over the UK changes between different event sizes. For a 1-in-10-year event there is only an 8% probability of being affected by a single substorm, although this rises to 17% for a 1-in-30-year event. In these circumstances we would not expect to see more than a single substorm taking place, for which there is a very low probability.

Table IV. Estimated likelihood of very intense substorms over the UK

Scenario	Number of very intense substorms over UK			Total cases
	0	1	2	
1-in-10-year	22 (92%)	2 (8%)	0 (0%)	24
1-in-30-year	20 (83%)	4 (17%)	0 (0%)	24
1-in-100-year	7 (29%)	12 (50%)	5 (21%)	24

However, for a 1-in-100-year event the probability of being affected increases significantly. For example, there is a 50% probability that the UK would experience a very intense substorm, and a 21% probability of two very intense substorms, taking place across the nation's geographic area.

4.2. GIC vulnerability assessment

We find that the peak GIC per transformer phase (using 1-minute sampled data), ranges from a median of 2A and maximum of 20A in the 1-in-10-year scenario, to a median of 11A and a maximum of 156A in the most extreme 1-in-10,000-year scenario. The maximum GIC experienced per transformer phase is illustrated in Fig. 3A, showing some of the largest asset exposures are in the North East and North West of England. Appendix D provides detailed simulation summary statistics.

Fig. 3B illustrates the total GIC per node based on the EHV transformers present. The exposure was minimal for a 1-in-10-year event with a median of 2A and a maximum of 29A, whereas in the most

extreme event the median was 11A with a maximum of 245A. The difference between the median and the maximum exposure indicates large GICs flow in particular 'hot spots' at the eastern and western edges of the network. An interesting finding is that the magnitude of exposure is different between the GIC per transformer phase and total GIC per node (the former being of greater importance).

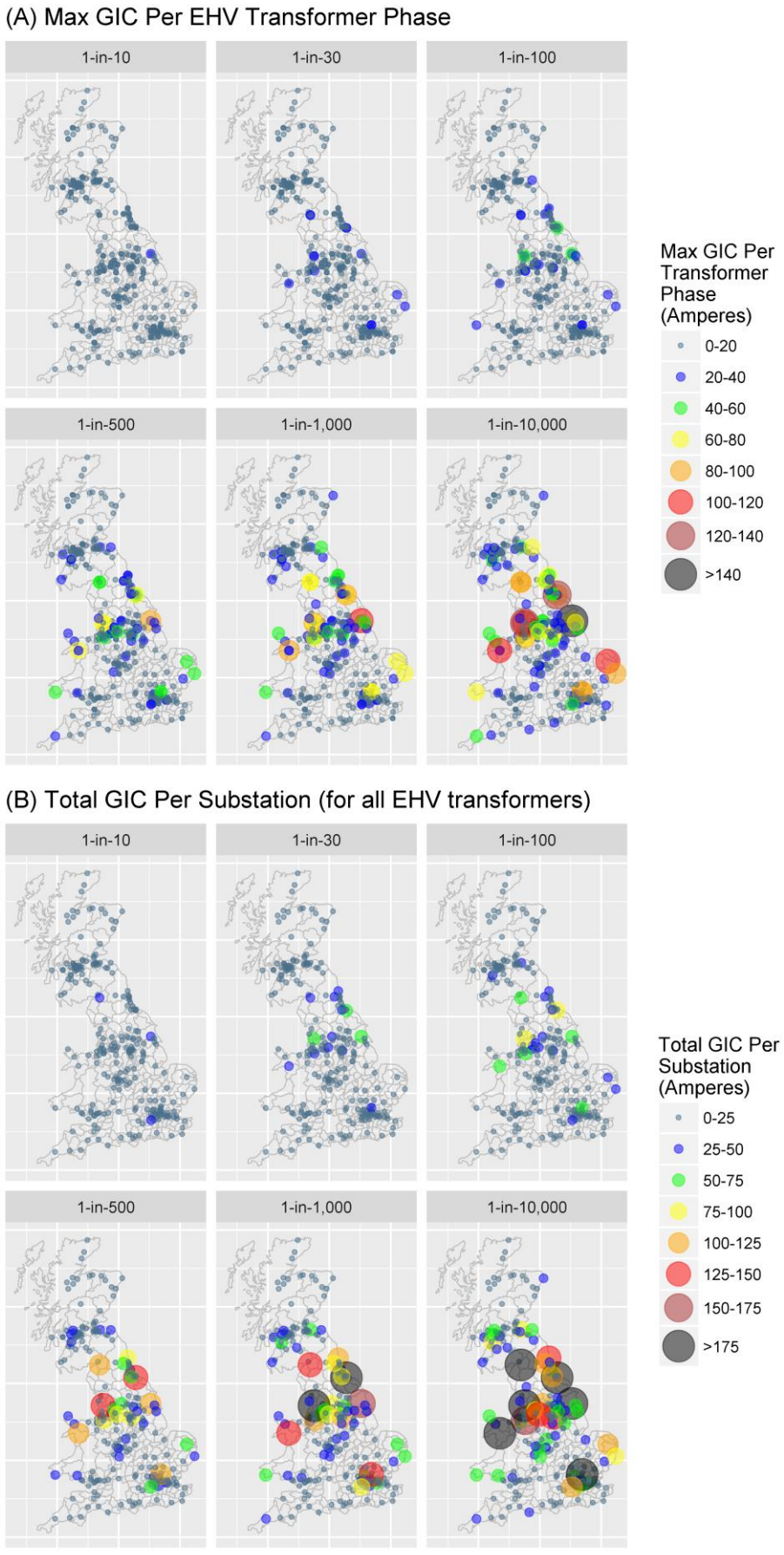

Fig. 3(A) Max GIC per EHV transformer phase and (B) Total GIC per substation

The frequency of failures based on the random allocation of unknown transformer characteristics are illustrated in Fig. 4A. The North East and North West of England had several transformers with a high frequency of failure, along with East Anglia and Wales. This is consistent with impacts reported during the 1989 storm, with transformer failure at Norwich (East Anglia) and significant transformer noise at Pembroke, South West Wales (Smith, 1990). No transformer damage takes place from a 1-in-10-year event, along with minimal impacts from a 1-in-30-year event. For the most probable extreme event, the 1-in-100-year scenario produced a transformer failure probability in at-risk nodes up to 5%. This increased to over 50% in the most extreme 1-in-10,000-year event.

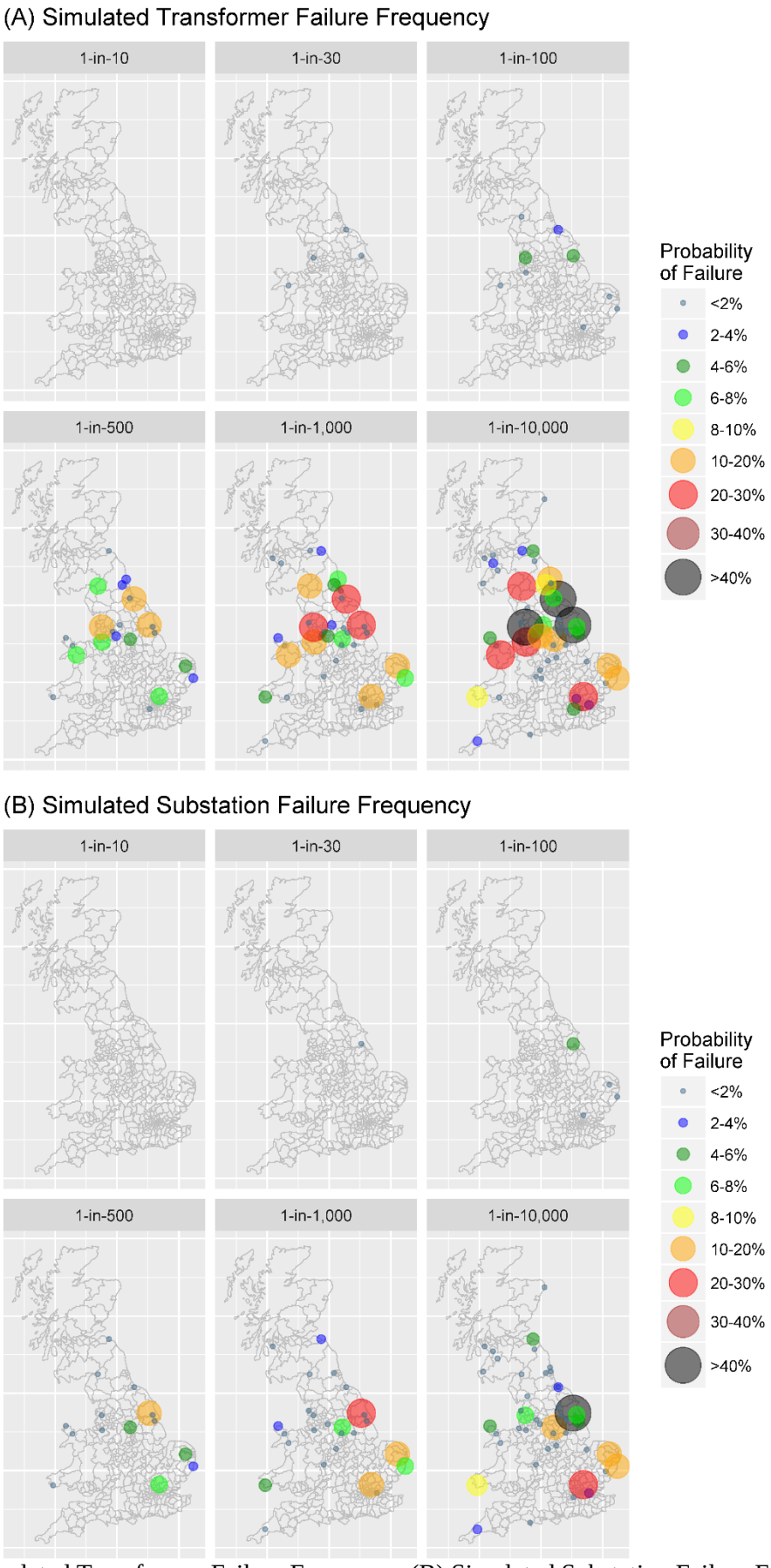

Fig. 4(A) Simulated Transformer Failure Frequency, (B) Simulated Substation Failure Frequency

However, a single transformer failure may not lead to the loss of the whole node. Consequently, we visualise the simulation results for the frequency of substation failure in Fig. 4B. Under these simulation conditions, it illustrates there is a small probability of power loss due to thermal heating, with the most vulnerable nodes generally positioned at the east and west coastal edges of the network. This probability ranges from 4% for the 1-in-100-year event up to over 40% for a 1-in-10,000-year event, with these effects at the eastern and western edges of the network, particularly at Sizewell, Norwich and Pembroke.

4.3. Socio-economic impact results

The direct impacts in the No Forecast scenarios were significantly higher when compared to other outcomes. In a 1-in-100-year event with No Forecast, initial disruption affected over 60 million people and almost 30 million workers. This impact is substantially reduced under the Current Forecast capability where direct population disruption dropped to 13 million and employment disruption dropped to 6 million. Enhanced forecasting capability reduced both population and labour disruption to a minimal level, particularly in smaller, more frequent events.

Table V details the level of population and labour disruption on day 1 of each scenario, as well as the consequential quarterly shock sizes applied to consumption and labour in the OEM macroeconomic model. We find that in a 1-in-100-year event with No Forecast, the GDP impact reached approximately £15.9 billion, with this dropping to £2.9 billion based on the Current Forecast capability, and £0.9 billion with an Enhanced Forecast. For a No Forecast, the 1-in-30-year event the GDP impact was £1.9 billion, decreasing to £0.4 billion under Current Forecast. Finally, for a 1-in-10-year event with no forecast the impact was £0.4 billion.

Table V. Economic impact by scenario

Event	Forecast Capability	Total Population Disruption (Millions) (Day 1)	Total Labour Disruption (Millions) (Day 1)	OEM Shock Type	OEM Shock	GDP loss (Billions, GBP)
1-in-100-year	**No Forecast**	62.1	29.4	Consumption	0.9518	15.9
				Labour	0.9527	
	Current Forecast	19.4	8.8	Consumption	0.9911	2.9
				Labour	0.9913	
	Enhanced Forecast	8.1	3.7	Consumption	0.9974	0.9
				Labour	0.9974	
1-in-30-year	**No Forecast**	13.3	6.1	Consumption	0.9942	1.9
				Labour	0.9944	
	Current Forecast	5.2	2.4	Consumption	0.9987	0.4
				Labour	0.9988	
	Enhanced Forecast	-	-	Consumption	-	-
				Labour	-	
1-in-10-year	**No Forecast**	5.2	1.4	Consumption	0.9987	0.4
				Labour	0.9993	
	Current Forecast	-	-	Consumption	-	-
				Labour	-	
	Enhanced Forecast	-	-	Consumption	-	-
				Labour	-	

5. DISCUSSION

Estimating the potential socio-economic impacts of space weather is a challenge as many areas of uncertainty exist, both in our current scientific and engineering understanding of this threat, and in current data and modelling methodologies. In this discussion we examine the findings of the analysis in relation to the research questions. Appendix E discusses the uncertainty associated with the data and modelling approaches utilised, and areas for future research.

What is the probability of CNI being affected by intense magnetospheric substorms?

Time sequences of substorms were constructed to estimate probabilities of geographic impact under different 1-in-10-year, 1-in-30-year and 1-in-100-year levels. Over a full 24-hour Earth rotation, the risk at any particular location is modest for the 1-in-10-year and 1-in-30-year events, but escalates markedly when we move to a 1-in-100-year event. Hence, we find that the UK was unlucky to experience the very intense substorm that caused two transformer failures during the 1989 event (the basis of the 1-in-30-year scenario) as the likelihood of geographic impact was only 17%, so it was a relatively rare but not improbable occurrence. Moreover, the results suggest it was entirely reasonable that the UK experienced no substorm, and consequently no power grid problems during the 2003 event (the basis of the 1-in-10-year scenario), as the substorm probability was only 8%.

Finally, we find that a Carrington-class event (the 1-in-100-year scenario) has a very high probability (71%) of producing very intense substorms over the UK that could disrupt the power grid, resulting from a 50% likelihood of a single very intense substorm and a 21% likelihood of two very intense substorms. In this latter case, the second event could occur many hours (perhaps 24 hours) after the initial event, thus posing a serious challenge to recovery efforts. During expert elicitation interviews it was expressed that two very intense substorms, particularly with no forecast available, would dramatically increase the probability of significant power grid difficulties, increasing the likelihood of a national grid collapse.

How vulnerable are specific electrical transmission CNI assets and nodes to GIC exposure?

As detailed data on transformer design characteristics are unavailable, we explored the sensitivity of transformer and node failure based on the random allocation of this parameter. Moreover, as there is little agreement regarding extreme events, we explore the sensitivity of the results to increasingly large geomagnetic storms.

Under the simulation conditions tested, the probability of transformer failure from thermal heating was generally quite low for more frequent events, but increased considerably in the more extreme scenarios, where the failure rate for some assets exceeded 50%. This translated to relatively modest impacts when evaluating the probability of node failure, as it would take more than half of the available EHV assets to fail for a blackout to be caused by the loss of a network node. Consequently, no nodes failed in the smaller, more frequent storm scenarios, but the failure probability ranged between 2-40% in the more extreme events. However, the actual failure rate depends on the asset management practices of the infrastructure operator, as the random allocation of transformer types introduces uncertainty in these results. For example, the model may overestimate the vulnerability of urban locations which are likely to be have been the focus of previous resilience efforts, while also underestimating the vulnerability of more rural substations. Either way, the results of this analysis provide evidence supporting grid configuration policies to place newer, more GIC-resistant designs at substations which contain transformers with older, less GIC-resistant designs. Finally, while the scenarios tested here have emphasised impacts at higher latitudes within the UK, such as the North East and North West of England, we must also avoid complacency about impacts in the South.

What are the potential socio-economic impacts of electrical transmission CNI failure due to space weather, under different forecasting capabilities?

Space weather forecasting is a recognised mitigation for managing the risk posed by space weather, and CNI operators are dependent on a forecast being available to take operational decisions to reduce exposure. The results were most concerning for the no forecast scenario, where the GDP impact reached almost £16 billion in the largest event. Given that space weather forecasting uses data from a limited number of satellites, some of which are nearing the end of the expected lifespan, this is concerning.

Many existing satellites are research missions (hence, effectively non-operational), and while high-quality data are collected, transmission to Earth may not take place in an optimal timeframe to support operational space weather forecasting.

The status-quo in terms of forecasting capability is unlikely to be maintained. Limited, or no investment, will see capability decline from today's skill levels, increasing the risk of CNI failure and consequential economic loss. Investment in the relevant space-borne monitoring is expected to lead to operationally reliable data streams that would achieve the enhanced capability described in Appendix C. Without this investment economic losses would be expected to be greater and fall somewhere between the current and no forecast capabilities. Based on the analysis presented here, there is evidence to support investment into maintaining forecasting capabilities, as well as predictive models and risk communication, as it provides early warning for the low probability, high impact threats caused by space weather. Importantly, the reduced economic impacts associated with better space weather forecasting capabilities depend on utilities having effective operational mitigation plans. While this is the case for the UK's National Grid, it might not apply in other regions where application of this risk framework may take place.

6. CONCLUSION

The time-shift analysis of the geomagnetic storm catalogue suggests that the UK risk is modest for the 1-in-10-year and 1-in-30-year levels, but significantly increases for a 1-in-100-year event. Moreover, in a sensitivity analysis of the vulnerability of transformer assets, we find the failure probability ranges from below 2% for minor events, to 4% for a Carrington-sized event approximately 1.4x larger than the 1989 event. The probability of substation failure ranged from negligible in smaller events, to over 40% based on the theoretical upper limit proposed by Vasyliūnas (2011).

We find that in a 1-in-100-year Carrington-sized event with no space weather forecasting capability, the GDP loss could be as high as £16 billion, with this figure dropping to £2.9 billion based on current forecasting capability. However, with existing satellites nearing the end of their life, current forecasting capability will decrease in coming years. Additional investment could provide enhanced forecasting, reducing the economic loss for a Carrington-sized 1-in-100-year event to £0.9 billion. We find that for a Carrington-sized 1-in-100-year event with no space weather forecasting capability, the GDP loss to the UK could be as high as £15.9 billion, with this figure dropping to £2.9 billion based on current forecasting capability. However, with existing satellites nearing the end of their life, current forecasting capability will decrease in coming years. Therefore, if no further investment takes place critical infrastructure will become more vulnerable to space weather. Additional investment could provide enhanced forecasting, reducing the economic loss for a Carrington-sized 1-in-100-year event to £0.9 billion.

Partial information often prevents comprehensive risk assessment. The contribution of this paper is to provide a general framework for the risk assessment of the socio-economic impacts of space weather for the UK. Applying this to the British high-voltage network forms one of the first socio-economic assessments undertaken for this threat (however, application to other countries would require further adaptation). Unlike other analyses undertaken hitherto, we properly address the general geophysical risk, asset vulnerability and CNI network structure. This has required a multidisciplinary approach, utilising methods from space physics, geophysics, electrical engineering and economics, but provides

a step towards the standardisation of space weather risk assessment. Importantly, we were conservative in our treatment of the space and geophysical hazard, estimating potential minimum impacts.

Further research must enhance this simulation to encompass the relationship between GIC, reactive power demand, and the available capacity (and critical paths) of spinning reserve under different forecasting capabilities. Future analyses should attempt to quantify the impact (and financial cost) of infrastructure 'hardening' via retrofitting. Finally, to capture the true socio-economic impacts space weather, disruption in other interdependent infrastructure systems must also be quantified, potentially increasing the economic impacts presented here.

Appendix A Detailed methodology on defining the space threat

This appendix outlines how we have developed simple scenarios to explore the impact of space weather on power grids in countries at high and mid-latitudes, regions where the strongest GICs are thought to be associated with magnetospheric substorms (Ngwira et al. 2015; Pulkkinen, Bernabeu, Eichner, Viljanen and Ngwira, 2015). These substorms are a fundamental dynamical cycle of Earth's magnetosphere, in which energy is extracted from the solar wind, stored in the tail of the magnetosphere and then explosively released (Dungey, 1961), each cycle typically lasting one to two hours, repeating as long as there is a supply of energy from the solar wind. Much of the explosive energy release is directed to Earth where it can produce a burst of intense aurora and electric currents in the upper atmosphere, leading to large geomagnetic variations which can spread from high to mid-latitudes during intense events. A geomagnetic storm typically contains a series of substorms and thus has the potential to produce a series of bursts of GIC in power grids.

Substorms are typically characterised using the auroral electrojet indices, a set of indices derived from geomagnetic measurements at 13 observatories in the northern hemisphere auroral zone, which monitor the electric currents (electrojets) flowing in Earth's ionosphere at auroral latitudes (Davis & Sugiura, 1966). Therefore, we have built our scenarios using values of these indices for two of the largest space weather events in recent decades, namely the geomagnetic storms of March 1989 and October 2003. We specifically focus on the AE index which represents the overall activity of the electrojets. Other indices such as AU and AL represent the strongest eastward and westward currents in the electrojets and are of interest for future studies, but in this first study we focus on AE.

Fig. A1 shows AE data for the March 1989 storm. The raw AE data is quite spikey as shown by the grey trace in the background. To highlight substorms, rather than short-lived features, we have smoothed these data with a 31-min running median (time-tagged to the central data point in each median). The use of a 31-minute window highlights variation in substorm timescales of 1-2 hours and use of a median ensures a focus on general trends that is not influenced by isolated extreme values. The smoothed AE for March 1989 is shown by the blue trace in Fig. A1. The main storm started at 01:27 UTC on 13 March. The event is marked by a vertical green line and indicates the arrival at Earth of a

major CME, one whose impact significantly compressed the geomagnetic field, a compression observed by ground-based magnetometers across the world (Observatori de l'Ebre, 2018). Following the onset of the main storm AE showed high activity throughout the whole of 13 March and the morning of 14 March. The main storm was preceded by significant activity in AE late on both 12 and 14 March, reflecting that the main storm was the central part of a two-week period of intense space weather (Allen, Sauer, Frank and Reiff, 1989).

The high peaks in this AE sequence indicate substorms that had major space weather effects. For example, the peak during the morning of 13 March is associated with the voltage collapse of the Hydro-Québec power grid in Canada (Bolduc, 2002), whilst the peak during the evening of 14 March was associated with a spectacular auroral display over southern England. To extract a simple scenario from this sequence of AE peaks we need to do two things: (a) set a threshold that we use to select the most intense substorms, and (b) associate the geomagnetic footprints of those substorms with particular geographic regions (such that power grids in those regions will be at risk from GIC driven by the substorm).

For the threshold we have set this at AE > 1900 nT, giving us a total of three very intense substorms during the main storm, indicated in red in Fig. A1. This is a fairly arbitrary choice of threshold but does match a number of major space weather impacts and effects reported as noted in Fig. A1. Most obviously the Hydro-Québec voltage collapse on the morning of 13 March, as well as the tripping of two UK transformers as reported by Smith (1990) and Erinmez, Kappenman and Radasky (2002). An internal technical report on the 1989 storm by the then nationalised electricity generator shows that two transformers, one at Norwich in East Anglia and one at Indian Queens in Cornwall, tripped out during the very intense substorm early on 14 March. The Norwich transformer also tripped out during a substorm on the evening of 13 March, one peaking just below our 1900 nT threshold. This suggests that this threshold is conservative, and thus appropriate for our aim of not overstating the risk.

Fig. A1. Variation of the auroral electrojet index AE during the great geomagnetic storm of 13/14 March 1989, annotated to show occurrence of major GIC impacts.

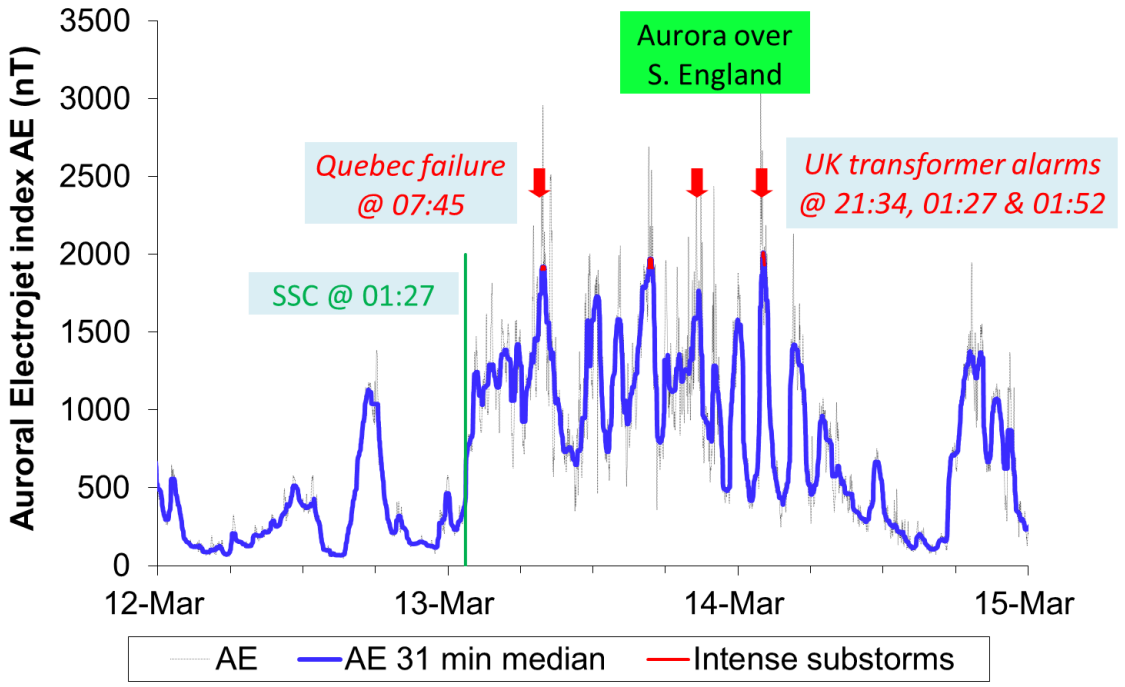

For the footprints we have set this at the region where local time near 02:30 at the time of the substorm. This was originally chosen to match the timing of the Hydro-Québec voltage collapse around 03:00 local time and the tripping of the two UK transformers, which was thought to have occurred during an intense substorm over southern England peaking around 02:00 local time. The latter speculation is now supported by recent access to the above report on UK power impacts, which confirms that the two transformers tripped between 01:20 and 02:00 local time. As noted above, that report also points to an additional trip during an earlier substorm, suggesting that a wider local window should be considered in future work. However, for the present work we focus the scenarios on a limited time window, which makes these scenarios fairly conservative in the assessment of space weather impacts on power grids. A wider window will require a more nuanced approach, e.g. a graduated weighting of impact by local time, for which we currently lack data.

This combination of AE thresholds and local time footprints allows us to build scenarios that are simply time sequences of intense substorms, each of which has a footprint in a particular time zone. Table AI below shows the scenario extracted from the AE data for the 1989 storm. As discussed in the main

paper we use this as our 1-in-30-year scenario, and also use a similar scenario derived from the October 2003 storm as our 1-in-10 year scenario.

Table AI. Substorm scenario derived from the 1989 scenario. Day 1 matches 13 March.

Day	*UTC at peak*	*Region at 02:30 local time*
1	07:55	Eastern Canada, North East US
1	16:45	Japan, SW Australia
2	02:05	Western Europe, including UK

To scale up to a 1-in-100-year scenario, we adapt detailed data from the March 1989 storm guided by the limited data from the storm of August/September 1859. This is widely considered as a 1-in-100-year space weather event, e.g. as in the collection of papers edited by Clauer & Siscoe (2006). Our knowledge of the 1859 event includes: (a) that it was a pair of geomagnetic storms, one large followed by an even larger event, (b) accurate times of the SSC for each storm (Stewart, 1861), and (c) an estimate of the Dst geomagnetic index for the larger storm (Siscoe et al. 2006). We use this knowledge to construct a representative AE timeline for the 1859 storm using two copies of the 1989 AE timeline. We time-shift each copy so that the Universal Time and day-of-year of the SSCs match those reported in Stewart (1861). We also increase the AE values in the second copy by a factor that reflects the greater strength of that storm. We derive that factor using estimates of the Dst index for the 1859 and 1989 storms (the AE index is available only from 1957). Although Dst is a measure of the storm severity, it is not a good measure of the auroral current systems. However, Dst is a good measure of the ring current. Since the repeated injection of particles towards the Earth during substorms contributes to the ring current, and in the absence of any better measurement, we have scaled the AE time series by the ratio of the Dst index between 1989 and 1859. We then use the resulting AE timeline to derive a 1-in-100-year scenario, which is shown in Table AII below.

Table AII 1-in-100-year substorm scenario. Day 1 matches 2 September

Day	*UTC at peak*	*Region at 02:30 local time*
-3	04:54	Atlantic Ocean
1	08:16	Eastern US and Canada
1	09:18	Central Canada and US
1	11:24	Pacific Ocean
1	15:05	New Zealand
1	15:52	Pacific Ocean
1	17:38	SE Australia, Japan
1	20:17	Central Siberia, Western China
2	00:16	European Russia
2	03:30	Atlantic Ocean
2	05:36	Atlantic Ocean
2	08:09	Eastern US and Canada
2	23:36	European Russia
3	12:47	Pacific Ocean, Alaska
6	18:28	Eastern China
7	17:11	SE Australia, Japan

We must emphasise that, in building this scenario, we have smoothed the AE index by a 31-minute running median so as to highlight substorms that re-occur on a timescale of a few hours Borovsky & Yakymenko (2017). However, we recognise that ionospheric currents that affect the power grid may occur on much shorter timescales and if we had used a shorter running median we would obtain a smoothed AE index with higher peaks (e.g. reducing the smoothing window size to 15 minutes increases peaks by 10 to 15%). Scaling by the Dst index could then imply greater disruption. At this stage of our research the link between AE and power grid effects is uncertain and therefore we have kept to our more conservative approach but note that the disruption could be even higher.

One striking thing about the 1-in-100-year scenario is that whilst the affected regions are spread around the world, there is only a very limited impact on Western Europe, including the UK. This is largely a consequence of the SSC time for the larger storm (05:00 on Day 1 of the 1-in-100-year scenario). To obtain a more realistic assessment of the 1-in-100-year impact on the UK we must consider a range of SSC times covering a full 24 hours of Universal Time, equivalent to a large CME arriving at any time of day. We do this quite simply by creating 24 instances of the scenario, with the SSC time stepped forward by 1 hour from one scenario to the next. We then analyse this ensemble of 24 instances to find how many scenarios give 0, 1 or more intense substorms over the UK with the results shown in the last row of Table A3 below. For comparison, we also apply this time-shift method to the 1-in-10 and 1-in-30-year scenarios.

Appendix B Detailed methodology on GIC estimation

We use a three-step process for computing GIC in EHV transmission infrastructure. The first step involves the measurement of the rapidly varying geomagnetic field using ground-based observatories. The second step is the computation of a map of the induced geoelectric field using either plane-wave or thin-sheet approximation (in which we use the latter here) from the interaction of the magnetic field with a ground conductivity model. The thin-sheet method has been validated against geoelectric field measurements in the UK and compares well with 3D conductivity models at periods longer than 1 minute. Finally, we utilise the topology, location and resistance characteristics of the electricity transmission infrastructure network model articulated in the previous section. This is placed onto the geoelectric field map to deduce the GIC (Beggan et al. 2013).

The spatial variation of the magnetic field was estimated using minute-mean data for the 1989 (as the 1-in-30-year exemplar and up-scaled by Dst for rarer events) and 2003 (1-in-10-year exemplar) storms, interpolated over a large region using the Spherical Elementary Current Systems method (Amm & Viljanen, 1999), as described in detail in McLay & Beggan (2010). The interaction of this rapidly varying magnetic field with the conductive Earth was then computed using the thin-sheet method (Vasseur & Weidelt, 1977). This determined the surface electric field arising at a particular frequency from layers of conductive material in the subsurface. The chosen frequency (or period) of the rate-of-change of the magnetic field is related to its penetration depth, which in this study is 600 seconds; a value that has been validated against measured electric field and GIC data where short-period local fluctuations are removed to leave the regional scale data (McKay, 2004).

The UK 2D surface conductance model is derived from the analysis of the conductivity properties of bedrock, based on the British Geological Survey 1:625,000 geological map of Great Britain. The model, described by Beamish & White (2012), uses information obtained from airborne geophysical surveys across the UK to determine the conductance to a depth of 3 km for the thin-sheet part of the model. For the offshore regions, the bathymetry and a uniform value of sea water conductivity (4 S/m) are used to determine conductivity. Fig. A2 illustrates the BGS2012 Conductance Model. At depth, below the thin-sheet model, a 1D model of resistivity down to 1000 km is used, based on information from

magnetotelluric studies of the UK (e.g. McKay, 2004). A national geophysical survey analogous to the US 'EarthScope' project is not available for the UK, though a current project to improve geophysical knowledge of the UK's conductivity structure is underway (SWIGS).

Fig. A2 BGS2012 Conductance Model 2D map for the top 3km of the crust

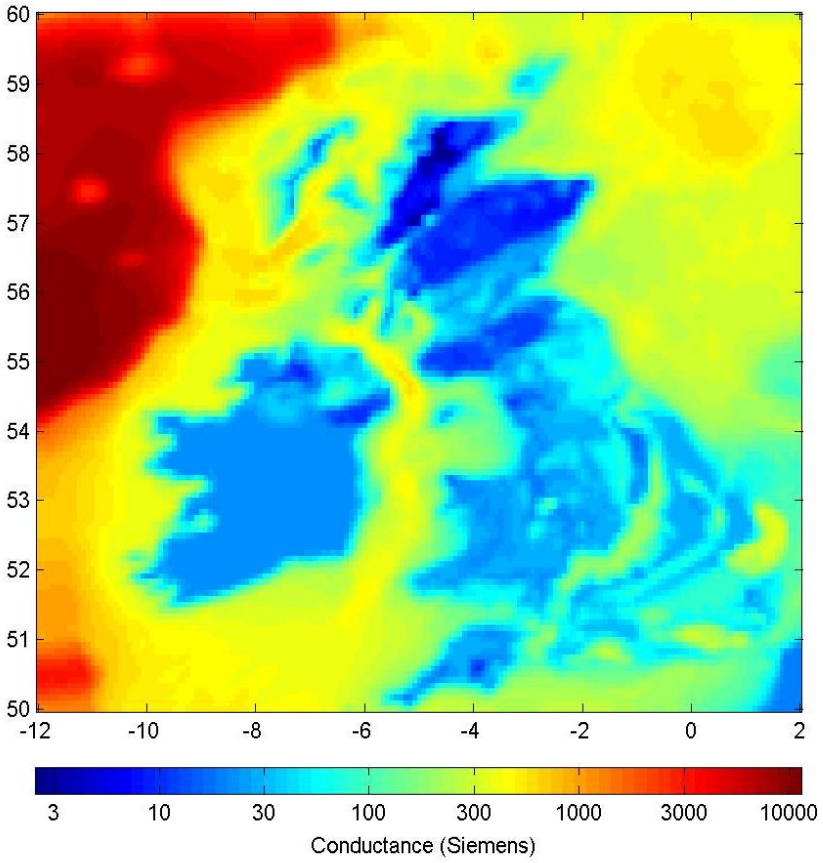

Appendix C Overview of space weather forecasting capabilities

Space weather forecasting can provide advanced warning to CNI operators that a solar storm has taken place on the surface of the Sun, and specific solar phenomena such as a CME may be directed at Earth. Data are used from a limited number of satellites, some of which are nearing the end of the expected lifespan, for example, some research satellites are already not considered operational. Whilst these research satellites collect high quality data, they may not be downloaded to Earth in an optimal timeframe to support operational space weather forecasting. As the implementation of operational mitigations by CNI operators has a substantial monetary cost associated, the confidence in the available forecast is an important variable.

The current level of capability depends on a mix of research and operational satellites which include DSCOVR, SOHO, and Advanced Composition Explorer (ACE) orbiting the Sun with the Earth. They are in direct line between the Sun and the Earth near the Lagrange 1 (L1) point where the combined gravitational attraction of the Sun and Earth allows quasi-stable satellite orbits. Quasi-stable orbits also exist at four other Lagrange point (L2 to L5) related to the Sun and Earth as shown in Fig. A3. The Geostationary Operational Environmental Satellites (GOES) exist along with SDO in near-Earth orbit and additionally STEREO A which is trailing the Earth, currently in a 1AU solar orbit at approximately 120° (halfway between L5 and L3).

Fig. A3 Lagrange positions

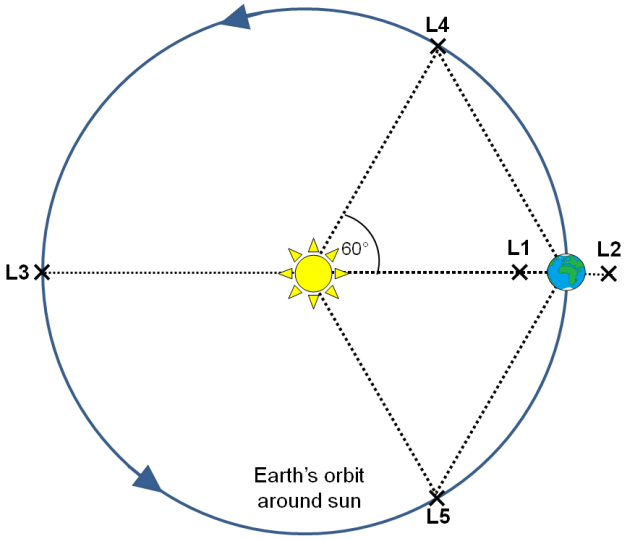

Current forecast capability allows complex sunspot regions to be identified 3-4 days before the Earth is in the direct line of any CMEs the region may produce. Any CME would then be detected by imagers on SOHO and STEREO A shortly after launch and the magnetic polarity of the CME 15-20 minutes (for a very fast CME) warning from in-situ measurements by DSCOVR/ACE at L1 point.

An enhanced level of forecasting would reflect the launching of an additional L5 satellite mission alongside a replacement L1 mission both providing operationally reliable data streams. The L5 mission would increase the lead time for identifying and monitoring complex active regions by a further 3 to 4 days and would provide a permanent side-on view of the interplanetary space between the Sun and Earth. This capability would improve the level of reliability and hence confidence in space weather forecasts, increasing the likelihood that infrastructure operators would take the appropriate operational mitigations when a threat is posed.

Appendix D Model summary statistics

Scenario	Type	Minimum (Amps)	Lower quartile (Amps)	Median (Amps)	Upper quartile (Amps)	Maximum (Amps)	Mean (Amps)	Standard deviation (Amps)
1-in-10	**Transformer**	0	1	2	4	20	3	3
1-in-30	**Transformer**	0	1	3	5	37	4	5
1-in-100	**Transformer**	0	1	4	7	52	6	8
1-in-500	**Transformer**	0	2	6	13	89	11	13
1-in-1,000	**Transformer**	0	3	8	16	115	14	17
1-in-10,000	**Transformer**	0	4	11	22	156	19	23
1-in-10	**Node**	0	1	2	4	29	4	5
1-in-30	**Node**	0	1	3	7	58	6	9
1-in-100	**Node**	0	1	4	9	82	9	13
1-in-500	**Node**	0	2	6	16	140	15	23
1-in-1,000	**Node**	0	3	8	20	181	19	29
1-in-10,000	**Node**	0	4	11	28	245	26	40

Appendix E Key data and modelling uncertainties

Space Threat

The key limitation relates to whether the past is a good predictor of the future, especially as we have been conservative in our estimates. For example, these probabilities are based on the analysis of the historical storm catalogue, but we know that we regularly see events which considerably exceed expected maximum values, with a recent example being the Fukushima nuclear power plant disaster in Japan. In this event, a tsunami wave exceeding 13 meters breached the plant's sea wall defences and led to one of the worst nuclear disasters in history. The tsunami considerably exceeded the maximum expected wave height. This was seen in advance of the disaster as a highly improbable event based on historical data (>1-in-10,000-year), hence why defences had not been engineered to withstand a tsunami of this magnitude. Future research needs to extend the analysis to encompass AE time-series values for the large events prior to 1989, such as 1959, 1960 and 1967.

Network Structure

The electricity transmission infrastructure network model used is a simplification of the actual network, along with the strict definition of node 'failure'. Modelling the lower voltage electricity distribution network was beyond the scope of this analysis, but doing so would capture the fact distribution nodes (e.g. 132 kV) sometimes have multiple connections to the transmission grid, increasing their level of resilience. Further research should consider using a DC power flow model for the transmission grid, providing more realistic representation of nodes that serve major power plants (e.g. Sizewell), as the loss of these nodes could have much wider system impacts.

Ground threat risk manifestation

When estimating ground conductivity in the UK, the existing state-of-the-art does not yet include 3D ground conductivity modelling. Although data collection efforts are now underway, it is likely to be a few years before enough data are collected to enable this endeavour to begin. In terms of objective validation, the BGS2012 model utilised a thin-sheet approximation that has been verified against measurements of the electric field at Lerwick, Eskdalemuir and Hartland observatories. The analysis

presented here is consistent with (Beggan, 2015) whereby the sensitivity of GIC modelling to variable ground conductivity was explored, in which the conclusion was that ground conductivity is a second-order effect and is only significant in around 10% of nodes.

Vulnerability assessment

A limitation of the vulnerability assessment undertaken is that it fails to address reactive power demand and voltage instability risk with the same level of rigour as thermal heating risk. Hence further research needs to attempt to scale the probability of voltage instability based on the reactive power demand in each system area.

Moreover, obtaining further geographical information from National Grid regarding the transformer design characteristics between urban and rural areas could help to refine the vulnerability assessment. In this analysis transformer designs were allocated randomly, however it is likely that assets with lower GIC thresholds exist at the rural edges of the network, where asset replacement is a slower process due to the limited number of customers served per node. In this analysis, the simulation results per node mean we end up with approximately 250,000 people per affected substation on average, which is higher than the 100,000 stated in the National Risk Register. This weakness results from using publicly available data, but further refinement of the simulation conditions could help to address this.

Resilience measures

The current approach to estimating the level of resilience gained from space weather forecasting is relatively qualitative, therefore further analysis should explore the potential use of event trees for evaluating the benefits of different levels of early warning. This type of approach would enable the event stages in different scenarios to be identified, and the probabilities of different event paths to be parameterised by expert elicitation methods. Such an approach would better address the cost-benefit trade-off CNI operators face when dealing with low confidence levels in space weather forecasts.

Scenario specification

Much of the analysis that already exists, particularly in the grey literature, provides little transparent evidence for how key scenario parameters have been determined. Often the descriptions of the expected scenarios have been very qualitative and derived from expert elicitation as we lack evidence to help parameterise more extreme events. Moving towards improved estimation of temporal restoration processes is certainly required and a weakness which affects the entire field focusing on the socio-economic impacts of space weather. For example, Eastwood et al. (2017) make reference to the uncertainty associated with both the spatial and temporal impacts as this can have a dramatic effect on estimated outcomes.

REFERENCES

Abt Associates. (2017). *Social and Economic Impacts of Space Weather in the United States*. Maryland, USA: Abt Associates for the National Oceanic and Atmospheric Administration. Retrieved from https://www.weather.gov/news/171212_spaceweatherreport

Albertson, V. D., Thorson, J. M., & Miske, S. A. (1974). The Effects of Geomagnetic Storms on Electrical Power Systems. *IEEE Transactions on Power Apparatus and Systems*, *PAS-93*(4), 1031–1044. https://doi.org/10.1109/TPAS.1974.294047

Allen, J., Sauer, H., Frank, L., & Reiff, P. (1989). Effects of the March 1989 solar activity. *Eos, Transactions American Geophysical Union*, *70*(46), 1479–1488. https://doi.org/10.1029/89EO00409

Amm, O., & Viljanen, A. (1999). Ionospheric disturbance magnetic field continuation from the ground to the ionosphere using spherical elementary current systems. *Earth, Planets and Space*, *51*(6), 431–440.

Baker, D. N., Li, X., Pulkkinen, A., Ngwira, C. M., Mays, M. L., Galvin, A. B., & Simunac, K. D. C. (2013). A major solar eruptive event in July 2012: Defining extreme space weather scenarios. *Space Weather*, *11*(10), 585–591.

Balan, N., Skoug, R., Tulasi Ram, S., Rajesh, P. K., Shiokawa, K., Otsuka, Y., … Nakamura, T. (2014). CME front and severe space weather. *Journal of Geophysical Research: Space Physics*, *119*(12), 2014JA020151. https://doi.org/10.1002/2014JA020151

Barnes, P. R., & Dyke, J. W. V. (1990). Economic consequences of geomagnetic storms (a summary). *IEEE Power Engineering Review*, *10*(11), 3–4. https://doi.org/10.1109/39.60450

Beggan, C. D. (2015). Sensitivity of geomagnetically induced currents to varying auroral electrojet and conductivity models. *Earth, Planets and Space*, *67*(1), 24. https://doi.org/10.1186/s40623-014-0168-9

Beggan, C. D., Beamish, D., Richards, A., Kelly, G. S., & P. Thomson, A. W. (2013). Prediction of extreme geomagnetically induced currents in the UK high-voltage network. *Space Weather*, *11*(7), 407–419. https://doi.org/10.1002/swe.20065

Bolduc, L. (2002). GIC observations and studies in the Hydro-Québec power system. *Journal of Atmospheric and Solar-Terrestrial Physics*, *64*(16), 1793–1802. https://doi.org/10.1016/S1364-6826(02)00128-1

Bolduc, L., Gaudreau, A., & Dutil, A. (2000). Saturation time of transformers under dc excitation. *Electric Power Systems Research*, *56*(2), 95–102. https://doi.org/10.1016/S0378-7796(00)00087-0

Bolduc, L., Langlois, P., Boteler, D., & Pirjola, R. (1998). A study of geoelectromagnetic disturbances in Quebec. I. General results. *IEEE Transactions on Power Delivery*, *13*(4), 1251–1256. https://doi.org/10.1109/61.714492

Borovsky, J. E., & Yakymenko, K. (2017). Substorm occurrence rates, substorm recurrence times, and solar wind structure. *Journal of Geophysical Research: Space Physics*, *122*(3), 2973–2998. https://doi.org/10.1002/2016JA023625

Boteler, D. (2014). Methodology for simulation of geomagnetically induced currents in power systems. *Journal of Space Weather and Space Climate*, *4*, A21. https://doi.org/10.1051/swsc/2014018

Boteler, D. H. (2006). The super storms of August/September 1859 and their effects on the telegraph system. *Advances in Space Research*, *38*(2), 159–172. https://doi.org/10.1016/j.asr.2006.01.013

Boteler, D. H., & Pirjola, R. J. (2014). Comparison of methods for modelling geomagnetically induced currents. *Ann. Geophys.*, *32*(9), 1177–1187. https://doi.org/10.5194/angeo-32-1177-2014

Boteler, D. H., Shier, R. M., Watanabe, T., & Horita, R. E. (1989). Effects of geomagnetically induced currents in the BC Hydro 500 kV system. *IEEE Transactions on Power Delivery*, *4*(1), 818–823. https://doi.org/10.1109/61.19275

Cabinet Office. (2017). *National risk register of civil emergencies – 2017 edition*. London: Cabinet Office. Retrieved from https://www.gov.uk/government/publications/national-risk-register-of-civil-emergencies-2017-edition

Cabinet Office, & Department for Business, Innovation & Skills. (2015). *Space Weather Preparedness Strategy* (No. Version 2.1). London: Cabinet Office and BIS. Retrieved from https://www.gov.uk/government/uploads/system/uploads/attachment_data/file/449593/BIS-15-457-space-weather-preparedness-strategy.pdf

Cannon, P., Angling, M., Barclay, L., Curry, C., Dyer, C., Edwards, R., … others. (2013). *Extreme space weather: impacts on engineered systems and infrastructure*. Royal Academy of Engineering. Retrieved from http://eprints.lancs.ac.uk/id/eprint/64443

Clauer, C. R., & Siscoe, G. (2006). The great historical geomagnetic storm of 1859: A modern look. *Advances in Space Research*, *38*(2), 117–118. https://doi.org/10.1016/j.asr.2006.09.001

Cliver, E. W., & Dietrich, W. F. (2013). The 1859 space weather event revisited: limits of extreme activity. *Journal of Space Weather and Space Climate*, *3*, A31. https://doi.org/10.1051/swsc/2013053

Davis, T. N., & Sugiura, M. (1966). Auroral electrojet activity index AE and its universal time variations. *Journal of Geophysical Research*, *71*(3), 785–801. https://doi.org/10.1029/JZ071i003p00785

Dungey, J. W. (1961). Interplanetary Magnetic Field and the Auroral Zones. *Physical Review Letters*, *6*(2), 47–48. https://doi.org/10.1103/PhysRevLett.6.47

Eastwood, J. P., Biffis, E., Hapgood, M. A., Green, L., Bisi, M. M., Bentley, R. D., … Burnett, C. (2017). The Economic Impact of Space Weather: Where Do We Stand? *Risk Analysis*, n/a-n/a. https://doi.org/10.1111/risa.12765

Echer E., Gonzalez W. D., & Tsurutani B. T. (2008). Interplanetary conditions leading to superintense geomagnetic storms (Dst ≤ −250 nT) during solar cycle 23. *Geophysical Research Letters*, *35*(6). https://doi.org/10.1029/2007GL031755

Erinmez, I. A., Kappenman, J. G., & Radasky, W. A. (2002). Management of the geomagnetically induced current risks on the national grid company's electric power transmission system. *Journal of Atmospheric and Solar-Terrestrial Physics*, *64*(5–6), 743–756. https://doi.org/10.1016/S1364-6826(02)00036-6

Gaunt C. T. (2016). Why Space Weather Is Relevant to Electrical Power Systems. *Space Weather*, *14*(1), 2–9. https://doi.org/10.1002/2015SW001306

Green, J. L., & Boardsen, S. (2006). Duration and extent of the great auroral storm of 1859. *Advances in Space Research*, *38*(2), 130–135. https://doi.org/10.1016/j.asr.2005.08.054

Hapgood, M. A. (2011). Towards a scientific understanding of the risk from extreme space weather. *Advances in Space Research*, *47*(12), 2059–2072.

Henley, E. M., & Pope, E. C. D. (2017). Cost-Loss Analysis of Ensemble Solar Wind Forecasting: Space Weather Use of Terrestrial Weather Tools. *Space Weather*, *15*(12), 2017SW001758. https://doi.org/10.1002/2017SW001758

Horton, R., Boteler, D., Overbye, T. J., Pirjola, R., & Dugan, R. C. (2012). A Test Case for the Calculation of Geomagnetically Induced Currents. *IEEE Transactions on Power Delivery*, *27*(4), 2368–2373. https://doi.org/10.1109/TPWRD.2012.2206407

Hutchins, T. R., & Overbye, T. J. (2011). The effect of geomagnetic disturbances on the electric grid and appropriate mitigation strategies. In *North American Power Symposium (NAPS), 2011* (pp. 1–5). https://doi.org/10.1109/NAPS.2011.6025162

Jonas, S., Fronczyk, K., & Pratt, L. M. (2018). A Framework to Understand Extreme Space Weather Event Probability. *Risk Analysis*. https://doi.org/10.1111/risa.12981

Kappenman, J. G. (1996). Geomagnetic Storms and Their Impact on Power Systems. *IEEE Power Engineering Review*, *16*(5), 5-. https://doi.org/10.1109/MPER.1996.491910

Kataoka, R. (2013). Probability of occurrence of extreme magnetic storms. *Space Weather*, *11*(5), 214–218. https://doi.org/10.1002/swe.20044

Kelly, G. S., Viljanen, A., Beggan, C. D., & Thomson, A. W. P. (2017). Understanding GIC in the UK and French high-voltage transmission systems during severe magnetic storms. *Space Weather*, *15*(1), 99–114.

Krausmann, E., Andersson, E., Gibbs, M., & Murtagh, W. (2016). *Space weather & critical infrastructures: Findings and outlook* (No. EUR 28237 EN). Brussels: Joint Research Centre. Retrieved from http://publications.jrc.ec.europa.eu/repository/bitstream/JRC104231/space_weather_cover%2Breport_final.pdf

Lehtinen, M., & Pirjola, R. (1985). Currents produced in earthed conductor networks by geomagnetically-induced electric fields. *Ann. Geophys.*, *3*(4), 479–484.

Lloyd's of London. (2013). *Solar Storm Risk to the North American Electric Grid*. London: Lloyd's of London.

Lotz, S. I., & Danskin, D. W. (2017). Extreme Value Analysis of Induced Geoelectric Field in South Africa. *Space Weather*, *15*(10), 1347–1356. https://doi.org/10.1002/2017SW001662

Love, J. J., Rigler, E. J., Pulkkinen, A., & Riley, P. (2015). On the lognormality of historical magnetic storm intensity statistics: Implications for extreme-event probabilities. *Geophysical Research Letters*. Retrieved from http://onlinelibrary.wiley.com/doi/10.1002/2015GL064842/full

Marti, L., Rezaei-Zare, A., & Narang, A. (2013). Simulation of Transformer Hotspot Heating due to Geomagnetically Induced Currents. *IEEE Transactions on Power Delivery*, *28*(1), 320–327. https://doi.org/10.1109/TPWRD.2012.2224674

McKay, A. J. (2004). Geoelectric fields and geomagnetically induced currents in the United Kingdom.

McLay, S. A., & Beggan, C. D. (2010). Interpolation of externally-caused magnetic fields over large sparse arrays using Spherical Elementary Current Systems. In *Annales Geophysicae* (Vol. 28, p. 1795). Copernicus GmbH.

Molinski, T. S. (2002). Why utilities respect geomagnetically induced currents. *Journal of Atmospheric and Solar-Terrestrial Physics*, *64*(16), 1765–1778. https://doi.org/10.1016/S1364-6826(02)00126-8

Möstl, C., Rollett, T., Frahm, R. A., Liu, Y. D., Long, D. M., Colaninno, R. C., … Vršnak, B. (2015). Strong coronal channelling and interplanetary evolution of a solar storm up to Earth and Mars. *Nature Communications*, *6*, 7135. https://doi.org/10.1038/ncomms8135

NERC. (2012). Special Reliability Assessment Interim Report: Effects of Geomagnetic Disturbances on the Bulk Power System. *North American Electric Reliability Council*.

Ngwira, C. M., Pulkkinen, A. A., Bernabeu, E., Eichner, J., Viljanen, A., & Crowley, G. (2015). Characteristics of extreme geoelectric fields and their possible causes: Localized peak enhancements. *Geophysical Research Letters*, *42*(17), 2015GL065061. https://doi.org/10.1002/2015GL065061

North, D. W. (2017). Space Weather: Introducing a Survey Paper and a Recent Executive Order. *Risk Analysis*, *37*(2), 204–205. https://doi.org/10.1111/risa.12778

Observatori de l'Ebre. (2018). International service on rapid magnetic variations. Retrieved 13 April 2018, from http://www.aemet.es/es/eltiempo/prediccion/municipios/mostrarwidget/roquetes-id43133?w=g4p01110011ohmfffffw410z251x4f86d9t95b6e9r1s8n2

ONS. (2016). Nomis - Official Labour Market Statistics. Retrieved 31 March 2018, from https://www.nomisweb.co.uk/

Oughton, E., Copic, J., Skelton, A., Kesaite, V., Yeo, Z. Y., Ruffle, S. J., … Ralph, D. (2016). *Helios Solar Storm Scenario* (Cambridge Risk Framework Series). Cambridge: Cambridge Centre for Risk Studies.

Oughton, E. J., Skelton, A., Horne, R. B., Thomson, A. W. P., & Gaunt, C. T. (2017). Quantifying the daily economic impact of extreme space weather due to failure in electricity transmission infrastructure. *Space Weather*, *15*(1), 65–83. https://doi.org/10.1002/2016SW001491

Pulkkinen, A., Bernabeu, E., Eichner, J., Beggan, C., & Thomson, A. W. P. (2012). Generation of 100-year geomagnetically induced current scenarios. *Space Weather*, *10*(4), S04003. https://doi.org/10.1029/2011SW000750

Pulkkinen, A., Bernabeu, E., Thomson, A., Viljanen, A., Pirjola, R., Boteler, D., … MacAlester, M. (2017). Geomagnetically induced currents: Science, engineering, and applications readiness. *Space Weather*, *15*(7), 2016SW001501. https://doi.org/10.1002/2016SW001501

Pulkkinen, A., Lindahl, S., Viljanen, A., & Pirjola, R. (2005). Geomagnetic storm of 29–31 October 2003: Geomagnetically induced currents and their relation to problems in the Swedish high-voltage power transmission system. *Space Weather*, *3*(8), S08C03. https://doi.org/10.1029/2004SW000123

Pulkkinen, Antti, Bernabeu, E., Eichner, J., Viljanen, A., & Ngwira, C. (2015). Regional-scale high-latitude extreme geoelectric fields pertaining to geomagnetically induced currents. *Earth, Planets and Space*, *67*(1), 93. https://doi.org/10.1186/s40623-015-0255-6

PwC. (2016). *Space Weather Study Results*. London. Retrieved from http://esamultimedia.esa.int/docs/business_with_esa/Space_Weather_Cost_Benefit_Analysis_ESA_2016.pdf

Ribeiro, P., Vaquero, J. M., & Trigo, R. M. (2011). Geomagnetic records of Carrington's storm from Guatemala. *Journal of Atmospheric and Solar-Terrestrial Physics*, *73*(2–3), 308–315. https://doi.org/10.1016/j.jastp.2009.12.017

Richardson, G. S., & Beggan, C. D. (2017). *Validation of geomagnetically induced current modelling code* (Technical Report No. Technical Report IR/17/009). Edinburgh: British Geological Survey.

Riley, P. (2012). On the probability of occurrence of extreme space weather events. *Space Weather*, *10*(2), S02012. https://doi.org/10.1029/2011SW000734

Riley, P., Baker, D., Liu, Y. D., Verronen, P., Singer, H., & Güdel, M. (2018). Extreme Space Weather Events: From Cradle to Grave. *Space Science Reviews*, *214*(1), 21. https://doi.org/10.1007/s11214-017-0456-3

Riley, P., & Love, J. J. (2017). Extreme geomagnetic storms: Probabilistic forecasts and their uncertainties. *Space Weather*, *15*(1), 2016SW001470. https://doi.org/10.1002/2016SW001470

Rodger, C. J., Mac Manus, D. H., Dalzell, M., Thomson, A. W., Clarke, E., Petersen, T., … Divett, T. (2017). Long-Term Geomagnetically Induced Current Observations From New Zealand: Peak Current Estimates for Extreme Geomagnetic Storms. *Space Weather*, *15*(11), 1447–1460.

Roodman, D. (2015, June 29). The risk of geomagnetic storms to the grid: A preliminary review. Retrieved from https://davidroodman.com/david/The%20risk%20of%20geomagnetic%20storms%205%20dr.pdf

Saiz, E., Guerrero, A., Cid, C., Palacios, J., & Cerrato, Y. (2016). Searching for Carrington-like events and their signatures and triggers. *Journal of Space Weather and Space Climate*, *6*, A6. https://doi.org/10.1051/swsc/2016001

Schrijver, C. J., Dobbins, R., Murtagh, W., & Petrinec, S. M. (2014). Assessing the impact of space weather on the electric power grid based on insurance claims for industrial electrical equipment. *Space Weather*, *12*(7), 487–498. https://doi.org/10.1002/2014SW001066

Schrijver, C. J., Kauristie, K., Aylward, A. D., Denardini, C. M., Gibson, S. E., Glover, A., … Vilmer, N. (2015). Understanding space weather to shield society: A global road map for 2015–2025 commissioned by COSPAR and ILWS. *Advances in Space Research*, *55*(12), 2745–2807. https://doi.org/10.1016/j.asr.2015.03.023

Schulte in den Bäumen, H., Moran, D., Lenzen, M., Cairns, I., & Steenge, A. (2014). How severe space weather can disrupt global supply chains. *Nat. Hazards Earth Syst. Sci.*, *14*(10), 2749–2759. https://doi.org/10.5194/nhess-14-2749-2014

Silverman, S. M. (2006). Comparison of the aurora of September 1/2, 1859 with other great auroras. *Advances in Space Research*, *38*(2), 136–144. https://doi.org/10.1016/j.asr.2005.03.157

Siscoe, G., Crooker, N. U., & Clauer, C. R. (2006). Dst of the Carrington storm of 1859. *Advances in Space Research*, *38*(2), 173–179. https://doi.org/10.1016/j.asr.2005.02.102

Smith, P. (1990). Effects of geomagnetic disturbances on the national grid system. In *25th Universities Power Engineering Conference, Aberdeen, UK*.

Space Studies Board. (2008). *Severe Space Weather Events–Understanding Societal and Economic Impacts: A Workshop Report*. Washington D.C.: National Academies Press. Retrieved from https://books.google.co.uk/books?hl=en&lr=&id=RLi3G4P7fiIC&oi=fnd&pg=PR1&dq=Severe+Space+Weather+Events+Understanding+Societal+and+Economic+Impacts::+A+Workshop+Report&ots=_cyJZNy5X9&sig=ivnVQiAxsXDN-f142VCzh8bsmXg

Stewart, B. (1861). XXII. On the great magnetic disturbance which extended from August 28 to September 7, 1859, as recorded by photography at the Kew Observatory. *Philosophical Transactions of the Royal Society of London*, *151*, 423–430.

Teisberg, T. J., & Weiher, R. F. (2000). Valuation of geomagnetic storm forecasts: an estimate of the net economic benefits of a satellite warning system. *Journal of Policy Analysis and Management*, *19*(2), 329–334.

Temmer, M., & Nitta, N. V. (2015). Interplanetary Propagation Behavior of the Fast Coronal Mass Ejection on 23 July 2012. *Solar Physics*, *290*(3), 919–932. https://doi.org/10.1007/s11207-014-0642-3

Thomson, A. W. P., Dawson, E. B., & Reay, S. J. (2011). Quantifying extreme behavior in geomagnetic activity. *Space Weather*, *9*(10), S10001. https://doi.org/10.1029/2011SW000696

Tosoni, E., Salo, A., & Zio, E. (2017). Scenario Analysis for the Safety Assessment of Nuclear Waste Repositories: A Critical Review. *Risk Analysis*.

Tsurutani, B. T., Gonzalez, W. D., Lakhina, G. S., & Alex, S. (2003). The extreme magnetic storm of 1–2 September 1859. *Journal of Geophysical Research: Space Physics*, *108*(A7), 1268. https://doi.org/10.1029/2002JA009504

Vasseur, G., & Weidelt, P. (1977). Bimodal electromagnetic induction in non-uniform thin sheets with an application to the northern Pyrenean induction anomaly. *Geophysical Journal International*, *51*(3), 669–690.

Vasyliūnas, V. M. (2011). The largest imaginable magnetic storm. *Journal of Atmospheric and Solar-Terrestrial Physics*, *73*(11–12), 1444–1446. https://doi.org/10.1016/j.jastp.2010.05.012

Viljanen, A., & Pirjola, R. (1994). Geomagnetically induced currents in the Finnish high-voltage power system. *Surveys in Geophysics*, *15*(4), 383–408. https://doi.org/10.1007/BF00665999

Webb, D. F., & Howard, T. A. (2012). Coronal Mass Ejections: Observations. *Living Reviews in Solar Physics*, *9*, 3.

White House. (2016, October 13). Executive Order -- Coordinating Efforts to Prepare the Nation for Space Weather Events. Retrieved 8 March 2018, from https://obamawhitehouse.archives.gov/the-press-office/2016/10/13/executive-order-coordinating-efforts-prepare-nation-space-weather-events